A TRIDENT SCHOLAR PROJECT REPORT

NO. 487

Many Body Systems of Coupled Dissipative Jaynes-Cummings Cavities

by

Midshipman 1/C Dean N. Rye, USN

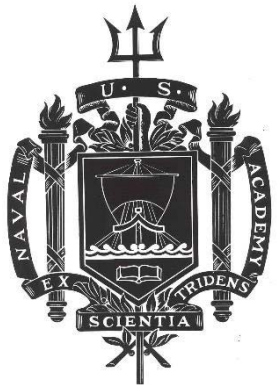

UNITED STATES NAVAL ACADEMY
ANNAPOLIS, MARYLAND

USNA-1531-2

REPORT DOCUMENTATION PAGE

Form Approved
OMB No. 0704-0188

1. REPORT DATE *(DD-MM-YYYY)*	**2. REPORT TYPE**	**3. DATES COVERED** *(From - To)*
5-20-19		

4. TITLE AND SUBTITLE
Many Body Systems of Coupled Dissipative Jaynes-Cummings Cavities

5a. CONTRACT NUMBER

5b. GRANT NUMBER

5c. PROGRAM ELEMENT NUMBER

6. AUTHOR(S)
Rye, Dean N.

5d. PROJECT NUMBER

5e. TASK NUMBER

5f. WORK UNIT NUMBER

7. PERFORMING ORGANIZATION NAME(S) AND ADDRESS(ES)

8. PERFORMING ORGANIZATION REPORT NUMBER

9. SPONSORING / MONITORING AGENCY NAME(S) AND ADDRESS(ES)
U.S. Naval Academy
Annapolis, MD 21402

10. SPONSOR/MONITOR'S ACRONYM(S)

11. SPONSOR/MONITOR'S REPORT NUMBER(S)
Trident Scholar Report no. 487 (2019)

12. DISTRIBUTION / AVAILABILITY STATEMENT

This document has been approved for public release; its distribution is UNLIMITED.

13. SUPPLEMENTARY NOTES

14. ABSTRACT

Open many body systems are difficult to solve because they obey non-equilibrium laws of physics. However, quantum many body systems are inherently coupled to the environment, necessitating a full understanding of non-equilibrium physics for real world applications. The Jaynes-Cummings model, consisting of a cavity with an atom interacting with a light field, provides a suitable platform to study many body non-equilibrium physics. In the single cavity, low photon states are achieved in the dispersive regime due to photon blockade, where the absorption of one photon blocks the absorption of a second. When open to the environment, the breakdown of this photon blockade sets in through dispersive bistability, where the cavity can reach two distinct stable solutions. We implement mean field theory to derive semiclassical equations which locate parameter regimes of bistability. Numerical solutions of the Lindblad master equation do not predict bistability directly, but unfolding the master equation into quantum trajectory calculations demonstrates switching between the semiclassical solutions. We then consider open systems of weakly interacting Jaynes-Cummings cavities. The bistability of the single cavity facilitates the emergence of symmetry-breaking states in multiple cavity systems, where the cavities achieve different steady states despite their coupling. Analysis of the two cavity system using quantum trajectories shows qualitative differences between symmetry-breaking and symmetry-preserving states. In the three cavity case, the symmetry-breaking bistability region extends past the critical point of typical symmetry-preserving bistability. The results for multiple Jaynes-Cummings cavities build towards a better understanding of open many body quantum physics.

15. SUBJECT TERMS
Quantum Physics, Cavity QED, Optical Bistability

16. SECURITY CLASSIFICATION OF:			**17. LIMITATION OF ABSTRACT**	**18. NUMBER OF PAGES**	**19a. NAME OF RESPONSIBLE PERSON**
a. REPORT	**b. ABSTRACT**	**c. THIS PAGE**		26	**19b. TELEPHONE NUMBER** *(include area code)*

U.S.N.A. --- Trident Scholar project report; no. 487 (2019)

Many Body Systems of Coupled Dissipative Jaynes-Cummings Cavities

by

Midshipman 1/C Dean N. Rye
United States Naval Academy
Annapolis, Maryland

_____
(signature)

Certification of Adviser(s) Approval

Assistant Professor Seth Rittenhouse
Physics Department

_____
(signature)

_____
(date)

Associate Professor Joel Helton
Physics Department

_____
(signature)

_____
(date)

Acceptance for the Trident Scholar Committee

Professor Maria J. Schroeder
Associate Director of Midshipman Research

_____
(signature)

_____
(date)

USNA-1531-2

Abstract

Open many body systems are difficult to solve because they obey non-equilibrium laws of physics. However, quantum many body systems are inherently coupled to the environment, necessitating a full understanding of non-equilibrium physics for real world applications. The Jaynes-Cummings model, consisting of a cavity with an atom interacting with a light field, provides a suitable platform to study many body non-equilibrium physics. In the single cavity, low photon states are achieved in the dispersive regime due to photon blockade, where the absorption of one photon blocks the absorption of a second. When open to the environment, the breakdown of this photon blockade sets in through dispersive bistability, where the cavity can reach two distinct stable solutions. We implement mean field theory to derive semiclassical equations which locate parameter regimes of bistability. Numerical solutions of the Lindblad master equation do not predict bistability directly, but unfolding the master equation into quantum trajectory calculations demonstrates switching between the semiclassical solutions. We then consider open systems of weakly interacting Jaynes-Cummings cavities. The bistability of the single cavity facilitates the emergence of symmetry-breaking states in multiple cavity systems, where the cavities achieve different steady states despite their coupling. Analysis of the two cavity system using quantum trajectories shows qualitative differences between symmetry-breaking and symmetry-preserving states. In the three cavity case, the symmetry-breaking bistability region extends past the critical point of typical symmetry-preserving bistability. The results for multiple Jaynes-Cummings cavities build towards a better understanding of open many body quantum physics.

Keywords: Quantum Physics, Cavity QED, Optical Bistability

Acknowledgments

I would like to thank my project advisors Professors Seth Rittenhouse and Joel Helton for their expertise and guidance leading up to and over the course of this project. I would also like to thank Professor Ryan Wilson, who piqued my interest in theoretical physics and set me down this research path over two years ago. Finally I would like to thank the Trident Committee here at the Naval Academy, as well as the Office of Naval Research, for the opportunity to embark on this research project.

Contents

I Introduction

Although the fundamental concepts behind quantum mechanics have been around for almost a century, there is still much to be learned about the physics of the extremely small. The laws of the subatomic world are difficult to comprehend because they do not agree with the classical laws of physics we experience and observe directly. Although they often defy common sense, the laws of quantum physics can be explained mathematically and have been demonstrated experimentally. Much of the technology we use today relies on our knowledge of quantum mechanics, which has improved vastly over the past few decades. As our knowledge of the fundamental laws of the subatomic world grows, so does our ability to use it for various applications.

For any realistic application of quantum mechanics, an open system must be considered where coupling occurs between the quantum system and its environment. This is because it is impossible to create a perfectly isolated, or closed, quantum system, even in heavily controlled laboratory experiments [1]. As a result, quantum systems typically lose their coherence on relatively short timescales. This decoherence is one of the largest obstacles to storing and manipulating information with quantum systems. While coupling to the environment is unavoidable and destroys coherence, over the past few decades the ability to control that system-environment coupling has vastly improved, especially in the field of quantum optics [2–6]. Studying these controlled open systems has led to the development of non-equilibrium laws of physics, as opposed to the typical equilibrium physics seen in closed and classical systems. In non-equilibrium physics, quantities such as energy and momentum are not necessarily conserved due to uncontrollable dissipation into the environment. In the absence of well-understood equilibrium laws, these systems difficult to understand and describe mathematically.

Of particular interest in this project is the application of non-equilibrium physics to a many body model, which describes a system of coupled quantum systems, which are each coupled to the environment through drive and dissipation as well. The Jaynes-Cummings (JC) model provides a useful platform for studying and understanding non-equilibrium physics for single and few-body models, and eventually a many body model. The JC model, which consists of photons and an atom coupled in a cavity, is particularly useful for exploring light-matter interactions [7]. Quantum phenomena exhibited by this model such as photon blockade and optical bistability have been studied and demonstrated experimentally [5–13]. The systems parameters which govern the behavior of the model have been examined in various limits, such as the strong and weak coupling regime or dispersive regime [8, 11]. The JC cavity in the strong-coupling regime has been proposed as an advantageous architecture for superconducting qubits for the purpose of quantum computation, due to experimental success in suppressing decoherence of the qubit while allowing one-bit operations [14]. The dynamics and properties of the two cavity JC dimer have also been examined, particularly the delocalization-localization dynamical phase transition in both equilibrium and non-equilibrium systems [3, 15].

Other quantum systems comparable to the JC model have been studied in the many body limit, such as the Bose-Hubbard and Dicke models [16–18]. Much of the focus of these studies has been on identifying quantum phase transitions in the absence of dissipation, such as between a Mott-insulating phase and a superfluid phase [19–21]. Circuits of microcavities have been realized experimentally in order to better understand these phases [22–26].

In the following, we explore the various properties of the single cavity JC model and how they are affected when scaled up to two cavity and three cavity system. Section II discusses the background and basic physics of the single JC cavity, including the simplest case of photon blockade. In Section III, the mathematical methods used throughout the paper are explained in detail. These methods are used to compare full quantum treatment using the master equation and quantum trajectories with mean field theory using semiclassical equations to provide a comprehensive description of the single cavity JC model in Section IV. The properties and characteristics of the single cavity are then explored for the JC dimer in Section V, which consists of two weakly interacting cavities. Results showing the emergence of symmetry-breaking states as a product of optical bistability are discussed. In Section VI, the three cavity array is described using semiclassical treatment, and we develop a phase diagram depicting bistability and symmetry-breaking behavior in the parameter space of cavity coupling and drive strength. The results for all three systems are summarized in Section VII.

II Background

A. Jaynes-Cummings Model

The JC model consists of a two-level atom that interacts with light inside a cavity. The light is assumed to be of a single mode with frequency ω_c, so that each photon has an energy of $E = \hbar\omega_c$, while the two energy levels of the atom are separated by $\Delta E_a = \hbar\omega_a$. As a two-state system, the atom can be

modeled with a spin-1/2 system, where spin up corresponds with the upper energy level and spin down corresponds with the lower energy level. The cavity light and atom exchange energy through the absorption and emission of photons. An atom in the spin down state can absorb a photon and transition to the spin up state, or an atom in the spin up state can emit a photon to the cavity light, transitioning to the spin down state. The rate of photon-spin exchange is reflected by the atom-light coupling coefficient g.

The Hamiltonian is an operator used in quantum mechanics to describe the total energy of a system. For the closed JC model, the total energy is a summation of three terms: the energy of the cavity light, the energy of the two-level atom, and the interaction energy between the atom and light. As an operator, the Hamiltonian is

$$\hat{H} = \hbar\omega_a\hat{\sigma}^+\hat{\sigma}^- + \hbar\omega_c\hat{a}^\dagger\hat{a} + \hbar g(\hat{a}^\dagger\hat{\sigma}^- + \hat{a}\hat{\sigma}^+) \quad (1)$$

The spin operators, $\hat{\sigma}^+$ and $\hat{\sigma}^-$, raise and lower the spin, or energy state, of the atom. The photonic creation and annihilation operators, $\hat{a}^\dagger$ and $\hat{a}$, add or remove a photon from the cavity light. The application of the raising and lowering operator on a state returns the value of the respective operators' observable. For example:

$$\begin{aligned}\hat{\sigma}^+\hat{\sigma}^-|n,s\rangle &= s|n,s\rangle \\ \hat{a}^\dagger\hat{a}|n,s\rangle &= n|n,s\rangle\end{aligned} \quad (2)$$

Where for a state $|n,s\rangle$, n is the number of photons in the cavity and s is the spin-state of the atom. The interaction term of the Hamiltonian comes from the exchange of energy between the atom and the light. The $\hat{a}^\dagger\hat{\sigma}^-$ term corresponds with the emission of a photon from the atom to the cavity light, and the $\hat{a}\hat{\sigma}^+$ term corresponds with the absorption of a photon from the cavity light to the atom.

Light-matter interactions can be studied in equilibrium using the closed JC model, as seen in for the JC dimer in Section V, but for realistic applications an open model must be understood. The system experiences loss through two decay channels: cavity loss when photons tunnel through the walls of the cavity, and spontaneous emission when the atom emits photons that do not enter the cavity field. To counter this dissipation, the cavity is driven with an external photon source such as a laser, with a drive strength reflected by the coefficient $\mathcal{E}$. The laser may have its own frequency, ω_d, separate from the cavity field and atom. The schematic for the driven-dissipative JC model is shown in Figure 1

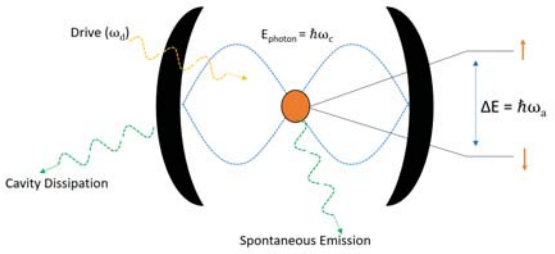

FIG. 1: Driven-Dissipative Jaynes Cummings Model: The cavity light and the two-state atom can exchange energy. The cavity is driven externally to add photons in order to counter dissipation from cavity loss and spontaneous emission

For the driven-dissipative model, it is convenient to use the interaction picture which drops rapidly oscillating terms that violate conservation of energy [8, 9]. The driven-dissipative Hamiltonian becomes

$$\begin{aligned}\hat{H}_{JC} &= \hbar\Delta\omega_a\hat{\sigma}^+\hat{\sigma}^- + \hbar\Delta\omega_c\hat{a}^\dagger\hat{a} \\ &+\hbar g(\hat{a}^\dagger\hat{\sigma}^- + \hat{a}\hat{\sigma}^+) + \hbar\mathcal{E}(\hat{a} + \hat{a}^\dagger)\end{aligned} \quad (3)$$

With the drive detunings $\Delta\omega_a = \omega_d - \omega_a$ and $\Delta\omega_c = \omega_d - \omega_c$. When the frequency of the atom matches the frequency of the cavity, $\omega_a = \omega_c$, the system is considered on resonance. Much of this paper will consider the on-resonance case, so that $\Delta\omega_c = \Delta\omega_a = \Delta\omega$. The system is dispersive if the detuning $\delta = \omega_c - \omega_a$ is nonzero. If the drive frequency matches that of the cavity, $\Delta\omega_c = 0$, the system is driven on resonance. Each of these regimes is considered at some point in this paper.

B. Photon Blockade

In certain parameter regimes of the JC model, the absorption of a single photon by the system can impede the absorption of additional photons. This concept, known as photon blockade, is seen in strongly nonlinear quantum optics systems, where the quantum energy ladder becomes anharmonic. This effect is easily understood in the closed system, with no drive or dissipation, and in the non-dispersive regime $\omega_c = \omega_a = \omega_0$. Diagonalization of the Hamiltonian, shown in Appendix A, produces energy doublets split by a factor of $\sqrt{n}\hbar g$. This means a cavity with n photons is either in an upper or lower state, and the energies of those states are:

$$\begin{aligned}E_{n,U} &= n\hbar\omega_0 + \sqrt{n}\hbar g \\ E_{n,L} &= n\hbar\omega_0 - \sqrt{n}\hbar g\end{aligned} \quad (4)$$

The splitting of these energy levels is dependent on the atom-light coupling strength, g. The nonlinear $\sqrt{n}$ splitting detunes the energy ladder of the system enough to prevent additional energy from entering

the system. The lowest levels of the energy ladder are shown in Figure 2, starting from a vacuum state with zero energy.

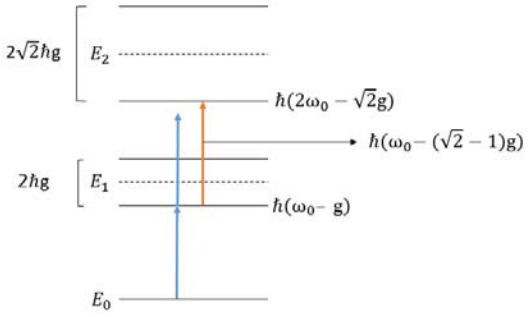

FIG. 2: Photon Blockade: The transition from E_0 to $E_{1,L}$ (blue) is detuned from the transition to $E_{2,L}$ (red) by a difference of $(2-\sqrt{2})\hbar g$

If a photon is to be added to the system, it must have a frequency matching a jump to another valid energy level. For the smallest possible jump, from E_0 to $E_{1,L}$, the photon must have a frequency of $\hbar(\omega_0 - g)$. The next jump, from $E_{1,L}$ to $E_{2,L}$, requires a photon of frequency $\hbar(\omega_0 - (\sqrt{2}-1)g)$. The difference between these two jumps, $\hbar(2-\sqrt{2})g$, prevents the absorption of a second photon for large coupling values relative to ω_0. A second photon with the same frequency as the one used to make the first jump will not be absorbed because it does not reach the next energy level.

The concept of photon blockade can be extended to a multiphoton blockade for states other than the vacuum state, higher on the energy ladder [8]. However, the effect of photon blockade is strongest for low photon numbers. Photon blockade occurs because the energy splitting for adjacent energy levels is different. However, for large n, the difference between $\sqrt{n}$ and $\sqrt{n+1}$ is negligible, so transitions between energy levels through the absorption of photons are not as restricted. This breakdown of photon blockade as a dissipative quantum phase transition is explored in Section IV and more thoroughly by Carmichael in Ref. [8]. The nonlinearity that results in photon blockade is an important characteristic of the JC model that also gives rise to optical bistability, as seen in Section IV.

III Methods

This paper utilizes three methods to analyze the behavior of JC cavities. First, the Lindblad master equation is used to evolve a density matrix to steady state. Then semiclassical mean field equations are used to determine steady states in the absence of quantum fluctuations. Finally quantum trajectories are used to demonstrate how quantum fluctuations cause switching between the semiclassical solutions in regimes where mean field theory applies.

A. Master Equation

The Hamiltonian is an effective tool by itself to describe a closed system, as it represents the total energy of the system. Open systems, however, lose energy to the environment, requiring another method to account for dissipation. Master equations evolve a density matrix ρ in time, which is defined as

$$\rho := \sum_{n,s} \rho_{n,s} |n,s\rangle\langle n,s| \tag{5}$$

Where the coefficients $\rho_{n,s}$ add up to one. Expectation values of the system, such as those for photon number and spin state, can be determined by taking the trace of the density matrix acted on by the appropriate operators. For example, the expectation value of the number of photons can be calculated as

$$\langle \hat{a}^\dagger \hat{a} \rangle = \langle \hat{n} \rangle = \mathrm{Tr}[\hat{a}^\dagger \hat{a} \rho] \tag{6}$$

Rather than describing an individual system, the density matrix represents an ensemble of identically prepared systems, so that observables extracted from the density matrix are an average expectation value of an ensemble. When a system has multiple steady states, such as in a bistable regime, the expectation values taken from its density matrix are averages of those states. Therefore the density matrix by itself cannot be used to locate bistable regions, or provide useful insight about the different steady states. Nevertheless, the master equation includes the effects of quantum fluctuations in its time propagation which makes it a valuable tool for describing open quantum systems such as the JC model.

The Lindblad master equation accounts for interactions between the system and its environment through dissipation. In the JC master equation, there are two dissipation terms: one for cavity loss at rate 2κ and one for spontaneous emission at rate γ. The resulting single JC model master equation, which we numerically solve using a fourth-order Runge-Kutta algorithm, is

$$\begin{aligned} \frac{d\rho}{dt} = \frac{1}{i\hbar}[\hat{H}_{JC}, \rho] + \kappa(2\hat{a}\rho\hat{a}^\dagger - \hat{a}^\dagger\hat{a}\rho - \rho\hat{a}^\dagger\hat{a}) \\ +\gamma/2(2\hat{\sigma}^-\rho\hat{\sigma}^+ - \hat{\sigma}^+\hat{\sigma}^-\rho - \rho\hat{\sigma}^+\hat{\sigma}^-) \end{aligned} \tag{7}$$

B. Semiclassical Equations

In addition to its shortcomings in providing insight about bistability, evolving the master equation becomes very inefficient for large systems with many possible states. The dimensions of the density matrix scale as $(2N)^m$ for m cavities truncated to a N photon maximum. The number of elements calculated for each time step grows exponentially with the photon maximum, and even faster with each additional cavity. In order to describe even two or three cavity systems truncated to relatively small photon numbers, the master equation becomes slow and inefficient. Since this paper aims to build towards understanding the many body JC model, other methods besides the master equation are required.

Rather than evolve a large density matrix until it reaches steady state, equations of motion for expectation values themselves can be derived through the implementation of mean field theory. The derivations of the equations of motion for the following three expectation values are shown in Appendix B: $\alpha = \langle \hat{a} \rangle, \beta = \langle \hat{\sigma}^- \rangle$, and $\zeta = \langle \hat{\sigma}_z \rangle$

$$\begin{aligned} \frac{d\alpha}{dt} &= -(\kappa - i\Delta\omega_c)\alpha - ig\beta - i\mathcal{E} \\ \frac{d\beta}{dt} &= -(\gamma/2 - i\Delta\omega_a)\beta + ig\alpha\zeta \\ \frac{d\zeta}{dt} &= -\gamma(\zeta + 1) + 2ig(\alpha^*\beta - \alpha\beta^*) \end{aligned} \tag{8}$$

Including the equations for the complex conjugates α^* and β^*, there are five equations that are solved to steady state, regardless of system size: a significant improvement over the master equation for systems with many photons or cavities (ζ is always real, so that $\zeta^* = \zeta$). However, mean field theory averages all quantum fluctuations, which means there is a trade off when using these semiclassical equations. Mean field theory cannot fully describe a quantum system, especially in parameter regimes where quantum fluctuations dominate. Regardless, these semiclassical equations provide insight into the nature of quantum systems, which can be enhanced when combined with insight from other methods such as evolving the master equation or quantum trajectories.

Much of this paper concentrates on the strong coupling regime, where atom-light coupling g is much larger than the dissipation rates κ and γ. In order to efficiently compare mean field theory solutions to the master equation, we assume cavity loss is the dominant decay channel, so $\gamma = 0$. Without spontaneous emission, the spin of the atom is conserved [8], so that $4|\beta|^2 + \zeta^2 = 1$. Eliminating ζ from the above equations, we have

$$\begin{aligned} \frac{d\alpha}{dt} &= -(\kappa - i\Delta\omega)\alpha - ig\beta - i\mathcal{E} \\ \frac{d\beta}{dt} &= i\Delta\omega\beta \pm ig\alpha\sqrt{1 - |\beta|^2} \end{aligned} \tag{9}$$

The on-resonance case is considered here, so that $\Delta\omega_c = \Delta\omega_a = \Delta\omega$. Setting these time derivatives to zero allows us to solve for their steady state values

$$\beta = \frac{\pm g\alpha}{\sqrt{\Delta\omega^2 + 4g|\alpha|^2}} \tag{10}$$

$$\alpha = \frac{-i\mathcal{E}}{\kappa - i(\Delta\omega \mp \frac{g^2}{\sqrt{\Delta\omega^2 + 4g^2|\alpha|^2}})} \tag{11}$$

The analytic steady state equations have two solutions, each stable in their own parameter regime. For positive drive detuning, $\Delta\omega > 0$, the top sign corresponds with the stable solution. For negative drive detuning, they are stable when the bottom sign is used. For large photon numbers, where the effects of photon blockade are negligible, an equation for mean photon number can be derived

$$n = \alpha^*\alpha = \frac{\mathcal{E}^2}{\kappa^2 + (\Delta\omega \mp \frac{g}{2\sqrt{n}})^2} \tag{12}$$

See Section II for other uses of the semiclassical equations for the single JC cavity.

C. Quantum Trajectories

An alternative to the master equation and semiclassical equations, quantum trajectories numerically simulate the dynamics of dissipative quantum systems. The time-propagation of the density matrix according to the master equation is really an ensemble of individual quantum trajectories. Rather than propagating a $(2N)^m$ by $(2N)^m$ matrix in time, an individual quantum trajectory propagates a state vector of size $(2N)^m$ in time. Although not explicitly shown here, the averaging of many quantum trajectories produces the same results of a master equation for the same quantum system [1]. Quantum trajectories in bistable regimes can exhibit switching between steady state solutions of the semiclassical equation, demonstrating agreement between mean field solutions and exact solutions with full quantum treatment through the master equation.

The Hamiltonian in Eq. (3) used in the master equation is Hermitian, an important requirement for non-dissipative systems. For the purposes of quantum trajectories, it is convenient to rewrite the master equation with a non-Hermitian Hamiltonian,

which includes dissipative terms that result in the depreciation of the wavefunction's norm $\langle\psi(t)|\psi(t)\rangle$

$$\frac{d\rho}{dt} = \frac{1}{i\hbar}\left[\hat{H}_{\text{eff}}\rho - \rho\hat{H}_{\text{eff}}^{\dagger}\right] + 2\kappa\hat{a}\rho\hat{a}^{\dagger} + \gamma\hat{\sigma}^{-}\rho\hat{\sigma}^{+} \quad (13)$$

$$\hat{H}_{\text{eff}} = \hat{H}_{JC} - \frac{i}{2}(2\kappa\hat{a}^{\dagger}\hat{a} + \gamma\hat{\sigma}^{+}\hat{\sigma}^{-}) \quad (14)$$

The effective Hamiltonian is then used to propagate a wavefunction, $|\psi(t)\rangle = |n, s\rangle$ according to the Schrodinger equation.

$$i\hbar\frac{d}{dt}|\psi(t)\rangle = \hat{H}_{\text{eff}}|\psi(t)\rangle \quad (15)$$

In this method, the operators in the dissipation terms are called jump operators, because they are used to model random quantum jumps [1]. As the wavefunction evolves according to the modified Schrodinger equation, quantum jumps occur where the wavefunction changes discontinuously. Since the effective Hamiltonian is non-Hermitian, the norm of the wavefunction $\langle\psi(t)|\psi(t)\rangle$ is not conserved, gradually decreasing from 1 to 0. The probability of a quantum jump occurring is related to the norm of the wavefunction in that the smaller the norm, the more likely a quantum jump will take place. To model this, a pseudo-randomly generated number r is generated between 0 and 1 and compared to the norm. When the norm falls below this number, a quantum jump occurs. If the wave function undergoes a photon number jump, the new state of the wavefunction becomes

$$|\psi(t)\rangle = \frac{\sqrt{(2\kappa)}\hat{a}|\psi(t)\rangle}{\langle\psi(t)|2\kappa\hat{a}^{\dagger}\hat{a}|\psi(t)\rangle} \quad (16)$$

Each quantum jump renormalizes the wavefunction, so that it evolves according to the modified Schrodinger equation again until the norm once again falls below a new randomly generated number, at which point another quantum jump occurs.

The norm decreases due to the non-Hermitian dissipation terms in the effective Hamiltonian. Systems with high dissipation rates will lose wavefunction normalization quicker than systems with low dissipation rates, depending on the state of the wavefunction. Therefore quantum jumps occur more often for systems with high dissipation rates. The likelihood of a given quantum jump occurring through a specific decay channel also depends on the dissipation rates. For the single JC model, there are only two possible jumps. The probabilities that a quantum jump is either through spontaneous emission P_s or cavity loss P_c are calculated in the following manner.

$$\begin{aligned} P_s &= \frac{\gamma\langle\psi(t)|\hat{\sigma}^{+}\hat{\sigma}^{-}|\psi(t)\rangle}{\gamma\langle\psi(t)|\hat{\sigma}^{+}\hat{\sigma}^{-}|\psi(t)\rangle + 2\kappa\langle\psi(t)|\hat{a}^{\dagger}\hat{a}|\psi(t)\rangle} \\ P_c &= \frac{2\kappa\langle\psi(t)|\hat{a}^{\dagger}\hat{a}|\psi(t)\rangle}{\gamma\langle\psi(t)|\hat{\sigma}^{+}\hat{\sigma}^{-}|\psi(t)\rangle + 2\kappa\langle\psi(t)|\hat{a}^{\dagger}\hat{a}|\psi(t)\rangle} \end{aligned} \quad (17)$$

Similar to determining when a quantum jump occurs, the type of quantum jump is determined by randomly generating a number between 0 and 1 and comparing it to one of the above probabilities. The jump then occurs according to Eq 16 for the jump operator chosen, and the process repeats.

Scaling quantum trajectories up to multiple cavities faces the same problems as the master equation, although to a lesser degree. Since individual trajectories only propagate a vector rather than a matrix, the number of calculations does not increase exponentially with system size. However, system size itself still increases exponentially with the number of cavities in the system, making quantum trajectories inefficient for systems with many cavities. True many body systems will primarily be modelled with mean field theory.

IV Single Cavity

A. Dissipative vs Non-Dissipative

Quantum systems are never truly isolated from the environment, which makes the study of open quantum systems important. Although the effects of dissipation cannot be eliminated, a major focus in quantum optics for the past three decades has been on controlling the coupling between quantum systems and the environment. Rather than attempt to fully isolate quantum systems, experiments have focused on manipulating the environment to drive systems into desired quantum states. Systems that are weakly coupled to the environment can be understood both experimentally and theoretically with the use of numerical methods such as the master equation and quantum trajectories. Comparison of dissipative and non-dissipative solutions for the single JC model are shown in Figure 3

For systems driven near resonance, there is a clear qualitative difference between the non-dissipative and dissipative solutions. The dissipative system tends towards a vacuum state with no photons as the drive frequency approaches resonance, while the non-dissipative system experiences a sharp increase in photon number. The dissipative system also exhibits peaks in photon number due to photon blockade. Single photon blockade, as discussed in Section II, occurs at $\Delta\omega = g = 50$. At such a low drive strength, the blockade effect causes a peak due to the easy absorption of the first photon, but does not allow for the absorption of more photons due to the

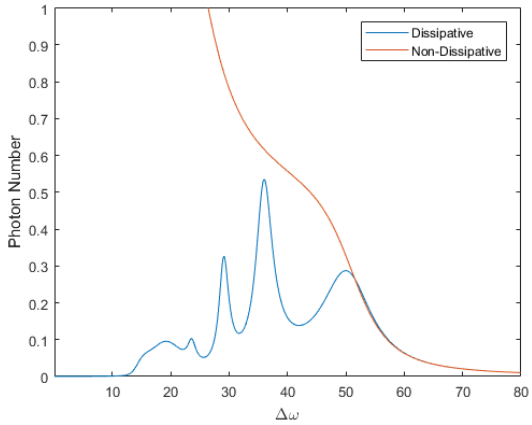

FIG. 3: Comparison of non-dissipative and dissipative solutions for $g = 50, \mathcal{E} = 5$. The dissipative solution was calculated using the master equation with $\kappa = 1, \gamma = 0$. Non-dissipative solution was calculated by solving for the ground state through diagonalizing the Hamiltonian.

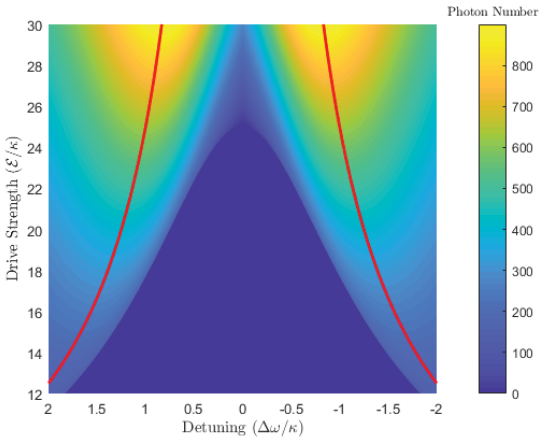

FIG. 4: Mean photon number as function of drive strength $\mathcal{E}/\kappa$ and detuning $\Delta\omega/\kappa$ for $g/\kappa = 50$. The red lines denote location of peak photon number for given drive strength, located at $\Delta\omega/\kappa = \pm\frac{g}{2\mathcal{E}}$

detuning from the next energy level. Each peak at lower values of $\Delta\omega$ also corresponds to a multiphoton blockade. For higher drive strengths and lower drive detunings, the multiphoton blockades begin to merge together into a blockade region, which separates high photon states from low photon states. In the absence of weak dissipation, the presence and effect of these multiphoton blockades would not be apparent. However, they are critical in understanding the phase transition from low to high photon number states, which is discussed below.

B. Dissipative Quantum Phase Transition

At higher drive strengths and lower drive detunings where $\Delta\omega$ is near 0, there is a sharp transition between the vacuum state and high photon number states. The region between these two states is dominated by a photon blockade region. Carmichael discusses a dissipative quantum phase transition in this region in detail [8]. The mean photon number calculated from Eq 12 is plotted as a function of drive strength and detuning in Figure 4, reaching excellent agreement with Carmichael's results from solving the Lindblad master equation to steady state. The red line marks the peak photon number for a given drive strength, located at $\Delta\omega/\kappa = \pm g/2\mathcal{E}$. The peak photon number is identical to that of an empty cavity with no atom, $n = (\mathcal{E}/\kappa)^2$.

Carmichael locates a critical point for zero drive detuning when $\mathcal{E}/\kappa = g/2 = 25$, where the energy spectrum of the system collapses from discrete levels to a continuous spectrum [8, 27]. Below this drive strength and driven slightly off resonance, a region of photon blockade separates the vacuum state with no photons from the high photon number states, as mentioned above. In this parameter regime, the transition from low photon number to high photon number states occurs through a cascade of multiphoton transitions that break down the blockade slowly. While the semiclassical equations fail to predict optical bistability as discussed in the next section, Carmichael provides evidence for the coexistence of the vacuum state and high photon number states in the region of photon blockade [8].

C. Bistability with Spontaneous Emission

The previous section assumed a resonant JC model, where $\Delta\omega_c = \Delta\omega_a = \Delta\omega$, and that spontaneous emission was negligible ($\gamma = 0$). Such conditions do not result in the typical absorptive optical bistability seen in cavity QED. Spontaneous emission from the atom to other modes besides that of the cavity breaks the conservation law that led to the self-consistent Equations (10), (11), and (12). The inclusion of spontaneous emission and the loss of spin conservation leads to a new analytic steady state equation for α [8]

$$\alpha = \frac{-i\mathcal{E}}{\kappa - i\Delta\omega + \frac{g^2(\gamma/2 + i\Delta\omega)}{\gamma^2/4 + \Delta\omega^2 + 2g^2|\alpha|^2})} \tag{18}$$

This equation can be rewritten as the typical state equation for the JC model, which relates the external drive strength to the number of photons in the cavity

$$\mathcal{E} = i\alpha(\kappa - i\Delta\omega + \frac{g^2(\gamma/2 + i\Delta\omega)}{\gamma^2/4 + \Delta\omega^2 + 2g^2|\alpha|^2}) \tag{19}$$

The state equation allows for multiple values of

α for a given drive strength $\mathcal{E}$. For certain parameter values, there can be as many as three possible solutions for a given drive strength, as seen in Figure 5. This region is one of optical bistability, as the high photon number and low photon number states are stable while the middle solution is unstable. It is important to note that bistability only occurs when drive and dissipation are included; the presence of two stable solutions as well as the ability to switch between them is due to interaction with the environment. The master equation is also shown to demonstrate agreement between the full quantum treatment of the master equation and the semiclassical equations derived from mean field theory which ignores quantum fluctuations.

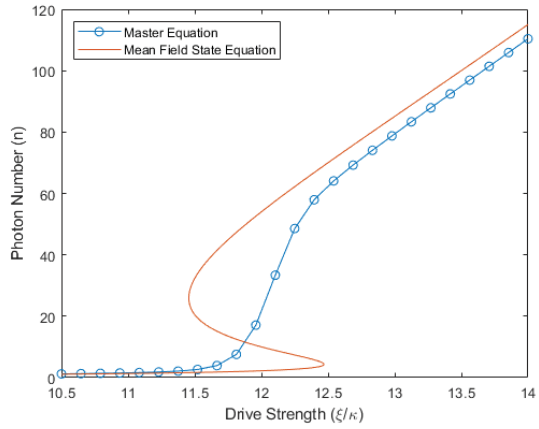

FIG. 5: Comparison of the state equation bistability curve to the master equation solutions for $g/\kappa = 30, \Delta\omega/\kappa = 0, \gamma/\kappa = 144$

While the master equation agrees with the state equation for drive strengths to the right and left of the bistability region, it cuts through the bistable solutions without displaying bistability itself. This is due to the nature of Lindblad master equation propagation, where the density matrix contains statistical information about an ensemble of identically prepared states that each undergo a stochastic process. Each state in the ensemble might exhibit switching between the bistable solutions at various times, with the steady state density matrix reflecting an average over states in the ensemble. Therefore the mean photon number according to the master equation is effectively a weighted average of the two stable solutions. Propagating the semiclassical equations, Eq. (8), recovers the same bistability as demonstrated by the state equation when initialized appropriately. A system initialized near the low photon number reaches its steady state at the lower solution, while a system initialized near the high photon number solution will stabilize at the higher solution. The middle solution, which is unstable, will never be reached by propagating the semiclassical equations.

In the absence of spontaneous emission, Carmichael explored the coexistence of two states where quantum fluctuations between the two states results in a mean photon number somewhere between the two states. In the regime considered by Carmichael, mean field theory fails to predict this coexistence of states [8]. However, with spontaneous emission turned on, the semiclassical equations accurately predict bistable solutions in the absence of quantum fluctuations.

D. Dispersive Bistability

Bistability is also observable in the dispersive regime, where $\Delta\omega_c \neq \Delta\omega_a$, or $\delta \neq 0$. In the strongly dispersive regime, where $\delta \gg g$, mean field predictions of bistability match up well with full quantum treatment. The state equation derived from the semiclassical equations of Eq. (8), when solved in terms of $\Delta\omega_c$ and δ, can be approximated well to the saturable extension of the Kerr model [8, 11]

$$\mathcal{E} = i\alpha(\kappa - i(\Delta\omega_c - \frac{g^2}{\delta}(1 + \frac{4g^2}{\delta^2}|\alpha|^2)^{-1/2}) \quad (20)$$

In this strongly dispersive regime, quantum trajectories using the method discussed in Section III display switching between the bistable solutions predicted by the state equation. An individual trajectory shown in Figure 6(c) demonstrates how quantum fluctuations induce switching between the two mean field solutions for a given drive strength.

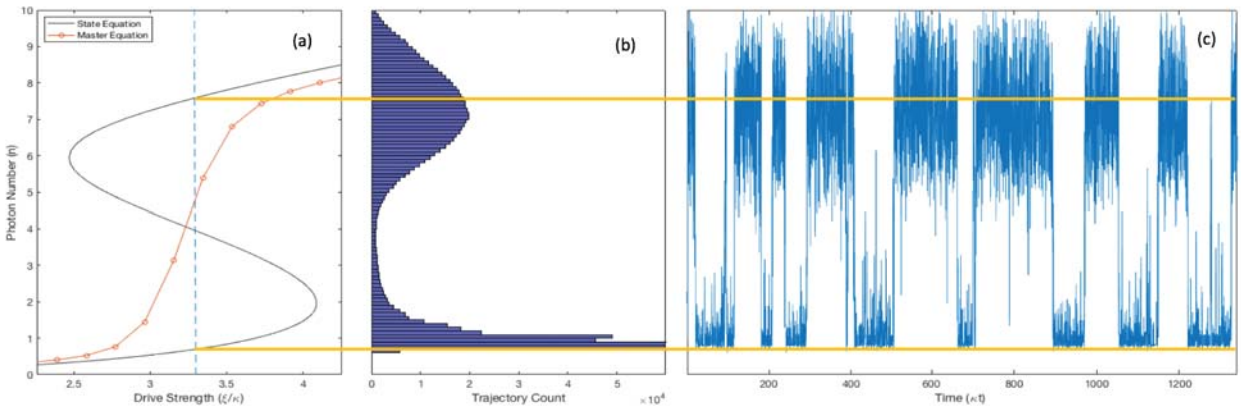

FIG. 6: (a) Semiclassical state equation compared with master equation for $\delta/\kappa = 1000$, $\Delta\omega_c/\kappa = 18$, $g/\kappa = 150$, $\gamma/\kappa = 0.084$ with the blue dashed line marking the drive strength used for the quantum trajectory shown in panels(b) and (c). (b) Distribution of photon number at each time step in single quantum trajectory with 500,000 time steps (c) Quantum trajectory for same parameters as panel (a) with $\mathcal{E}/\kappa = 3.3$. The yellow solid lines across all three figures give photon number stable solutions as predicted from the state equation for the parameters given

The mean field semiclassical solutions find excellent agreement with the full quantum solutions using the master equation and quantum trajectory. In this parameter regime, quantum fluctuations do not significantly affect the bistable solutions but rather cause flopping between them. Fluctuations in photon number oscillate more near the upper bistable solution due to coupling with the atom, while the lower bistable solution does not oscillate as much due to a near vacuum of photons, so that the atom cannot easily absorb and emit photons. The approximations made to develop the semiclassical and state equations results in only a slight overprediction of the upper solution and underprediction in the lower solution.

V Jaynes-Cummings Dimer

The next logical step in moving towards a many body model is describing a system of two coupled cavities, each with their own cavity field and two-level atom. This paper only considers inter-cavity coupling through the cavity fields, so that photons can effectively hop between cavities but the spins do not interact with each other directly. The dispersive bistability and bistability due to spontaneous emission are both extended to the two cavity model using the same methods as in Section IV, although the master equation and quantum trajectories take significantly longer to propagate. The bistable region in the two cavity region gives rise to symmetry-breaking states when the cavities are weakly coupled. Although the cavities are free to exchange photons, they reach two distinct steady states. Although quantum fluctuations still lead to switching between stable solutions as they did in the single JC model, the semiclassical equations show regions of stable symmetry-breaking states, effectively turning the bistable region into a multistable region with four stable solutions.

A. Expanded Hamiltonian and Operators

Before discussing the results and properties of the two cavity system, it's worth noting the effect of the combining states of two cavities on the operators and density matrix, as well as the methods discussed in Section III. The dimensions of the density matrix and all operators correspond to the number of combinations of all possible spin states (2 for each cavity), and photon number (up to the truncated number N for each cavity). In moving from a single cavity model to a two cavity model, the dimensions increase from a $(2N)^1$ by $(2N)^1$ matrix, to a $(2N)^2$ by $(2N)^2$ matrix. In order to compare mean field theory results with the master equation and quantum trajectories, this section focuses on parameter regimes with low photon numbers.

The Hamiltonian for all systems of made up of quantum elements is the summation of each individual element's Hamiltonian along with any interaction terms between them. In the two cavity JC system, the Hamiltonian becomes

$$\hat{H}_{2\text{cav}} = \hat{H}_1 + \hat{H}_2 - J(\hat{a}_2^\dagger \hat{a}_1 + \hat{a}_1^\dagger \hat{a}_2) \qquad (21)$$

The subscripts indicate which cavity the individual Hamiltonian is for, using either Eq. (1) for an

isolated system or Eq. (3) for a driven-dissipative system. The rate at which photons transfer between cavities is reflected by the cavity coupling J. The interaction terms make intuitive sense: $\hat{a}_2^\dagger \hat{a}_1$ adds a photon to cavity two and removes a photon from cavity one, and $\hat{a}_1^\dagger \hat{a}_2$ does the opposite.

The Lindblad master equation is developed in the same manner, with dissipation terms for cavity loss and spontaneous emission for both cavities.

$$\frac{d\rho}{dt} = \frac{1}{i\hbar}[\hat{H}_{2\text{cav}}, \rho] + \sum_{i=1,2} \kappa(2\hat{a}_i \rho \hat{a}_i^\dagger - \hat{a}_i^\dagger \hat{a}_i \rho - \rho \hat{a}_i^\dagger \hat{a}_i) + \sum_{i=1,2} \frac{\gamma}{2}(2\hat{\sigma}_i^- \rho \hat{\sigma}_i^+ - \hat{\sigma}_i^+ \hat{\sigma}_i^- \rho - \rho \hat{\sigma}_i^+ \hat{\sigma}_i^-) \tag{22}$$

The extension to the effective Hamiltonian used in quantum trajectories is straightforward as well, becoming

$$\hat{H}_{\text{eff,2cav}} = \hat{H}_{2\text{cav}} - \sum_{i=1,2} \frac{i}{2}(2\kappa \hat{a}_i^\dagger \hat{a}_i + \gamma \hat{\sigma}_i^+ \hat{\sigma}_i^-) \tag{23}$$

With four possible decay channels, the probabilities for four types of quantum jumps must be calculated instead of two. Once the norm falls below the randomly generated number, indicating a quantum jump, the probability of a quantum jump due to spontaneous emission in the first cavity is

$$P_{a1} = \frac{\gamma \langle \hat{\sigma}_1^+ \hat{\sigma}_1^- \rangle}{\gamma(\langle \hat{\sigma}_1^+ \hat{\sigma}_1^- \rangle + \langle \hat{\sigma}_2^+ \hat{\sigma}_2^- \rangle) + 2\kappa(\langle \hat{a}_1^\dagger \hat{a}_1 \rangle + \langle \hat{a}_2^\dagger \hat{a}_2 \rangle)} \tag{24}$$

Where expectation values are $\langle \hat{\sigma}_i^+ \hat{\sigma}_i^- \rangle = \langle \psi(t) | \hat{\sigma}_i^+ \hat{\sigma}_i^- | \psi(t) \rangle$ and $\langle \hat{a}_i^\dagger \hat{a}_i \rangle = \langle \psi(t) | \hat{a}_i^\dagger \hat{a}_i | \psi(t) \rangle$. Probabilities for the other three types of quantum jumps are calculated in the same manner.

The semiclassical equations change slightly, with an additional cavity coupling term in the equations for α_i. This method now solves for the steady states of ten equations, including the equations for the complex conjugates α_i^* and β_i^*. The semiclassical equations for cavity one are

$$\begin{aligned} \frac{d\alpha_1}{dt} &= -(\kappa - i\Delta\omega_c)\alpha_1 - ig\beta_1 - i\mathcal{E} - iJ\alpha_2 \\ \frac{d\beta_1}{dt} &= -(\gamma/2 - i\Delta\omega_a)\beta_1 + ig\alpha_1\zeta_1 \\ \frac{d\zeta_1}{dt} &= -\gamma(\zeta_1 + 1) + 2ig(\alpha_1^*\beta_1 - \alpha_1\beta_1^*) \end{aligned} \tag{25}$$

B. Equilibrium Dynamics

Understanding the equilibrium dynamics of the two cavity system gives some insight into the behavior of the driven-dissipative model. For the following dynamics, drive and dissipation are considered negligible, so that $\mathcal{E} = \kappa = \gamma = 0$. Without interaction with the environment, energy is conserved for the system. Energy can be stored in each cavity field and each atom, so that the conserved quantity is

$$\begin{aligned} N &= n_1 + n_2 + s_1 + s_2 \\ N &= \langle \hat{a}_1^\dagger \hat{a}_1 \rangle + \langle \hat{a}_2^\dagger \hat{a}_2 \rangle + \langle \hat{\sigma}_1^+ \hat{\sigma}_1^- \rangle + \langle \hat{\sigma}_2^+ \hat{\sigma}_2^- \rangle. \end{aligned} \tag{26}$$

Another useful quantity for the two cavity system is the photon imbalance, Z, which tracks the difference in photon numbers between the two cavities.

$$Z = \frac{n_1 - n_2}{N} \tag{27}$$

Z ranges from -1 to 1, where a value of 1 indicates all photons in the system are in cavity one and none are in cavity two, and a value of -1 indicates the opposite. Photon imbalance of $Z = 0$ indicates the photons are evenly distributed. This quantity is particularly useful for characterizing the localization of photons.

There are two competing coupling terms in the two cavity system: the atom-light coupling g, and the cavity coupling J. The equilibrium dynamics of the two cavity system are qualitatively different depending on which type of coupling dominates. The time evolution of photon imbalance for the strong atom-light coupling regime and weak atom-light coupling regime are compared in Figure 7

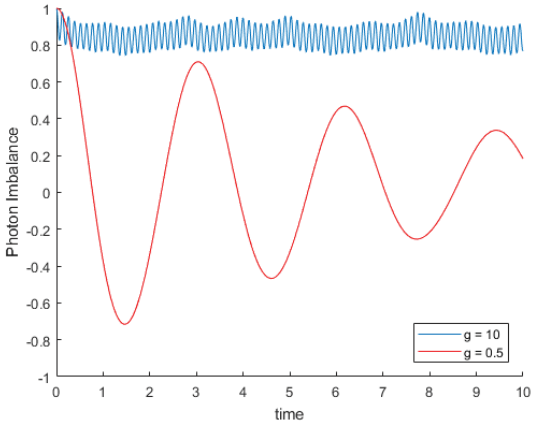

FIG. 7: Time evolution of photon imbalance for strong and weak atom-light coupling compared to cavity coupling for $\mathcal{E}/J = \kappa/J = 0, \omega_a = \omega_c = J$. System was initialized with $N = n1 = 6$ so that $Z_0 = 1$

When atom-light coupling dominates, the photons are effectively trapped in the first cavity. The rapid oscillations in photon imbalance are due to the exchange of energy between the first cavity's atom and

cavity field. The coupling between the cavity field and the atom prevents coupling between both cavity fields, so that photons cannot easily hop to the second cavity. On long time scales, the photon imbalance inverts so that all photons become trapped in the second cavity. However, these time scales are long enough that when compared to the weak atom-light coupling regime, the photons can be considered localized.

When the cavity coupling dominates, i.e. in the weak atom-light coupling regime, photons easily hop between cavities. There is still an exchange of energy between the cavity field and atom of each cavities, but the atom-light coupling is unable to "trap" the photons. Over long time scales, the photon imbalance continues to oscillate near a value of 0, so that the photons can be considered delocalized.

Since there are two dynamical states of photons, localized or delocalized, a dynamical phase transition can be identified between the weak and strong atom-light coupling regimes. This transition is analogous to the one studied in the many body JC and Bose-Hubbard models, where photons in the Mott-insulator phase are considered localized and photons in the superfluid phase are considered delocalized. When the time-averaged photon imbalance is plotted as a function of atom-light coupling, as shown in Figure 8, the transition from delocalized to localized photons is obvious. Schmidt *et al.* locate the phase transition at a critical value of g, also shown in Figure 8 [15]

$$g_{\text{crit}} \approx 2.8\sqrt{N}J \tag{28}$$

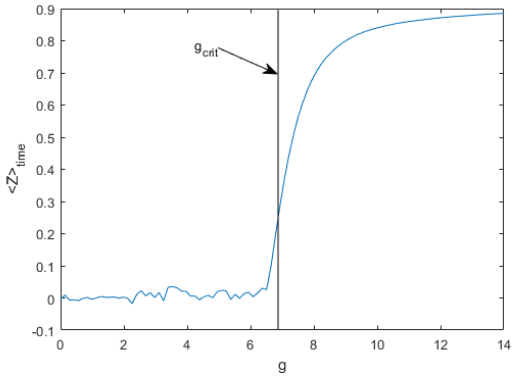

FIG. 8: Dynamical phase transition from delocalized to localized regimes. System was initialized with $N = n1 = 6$, *so that* $g_{crit}/J = 6.86$. *The discontinuities below* g_{crit} *are due to the effects of time averaging over relatively short time scales.*

Although these exact equilibrium dynamics may never be realized experimentally, they play a role in non-equilibrium steady states as well. The bistability seen in the single cavity is considered a product of the nonlinearity introduced to the system by the atom-light coupling g, as discussed in the photon blockade part of Section II. In this section, a different type of bistability occurs within the localized regime. The photons can either be trapped in one cavity or the other, giving two stable solutions, but only when g dominates. If these states are achieved as steady states of the driven-dissipative system, the symmetry of the system is considered broken. When the cavity coupling dominates, preventing photon localization, bistability and symmetry-breaking states should become unachievable in the driven-dissipative system.

C. Symmetry-Breaking Bistability

The optical bistability of the single JC model extends to the two cavity system for low cavity coupling values. Intuitively, symmetry-breaking states must arise from the bistable regions of the two cavity system, as there must be at least two possible solutions in order for the cavities to reach different steady states. Assuming no interaction between the cavities, $J = 0$, recovers the same bistability as the single cavity. When photon hopping is allowed, a two cavity state equation derived from the semiclassical equations predicts bistability as long as symmetry is preserved ($\alpha_1 = \alpha_2$). The symmetry-preserving state equations for non-dispersive and dispersive systems are

$$\begin{aligned}\mathcal{E} &= i\alpha(\kappa - i(\Delta\omega - J) + \frac{g^2(\gamma/2 + i\Delta\omega)}{\gamma^2/4 + \Delta\omega^2 + 2g^2|\alpha|^2}) \\ \mathcal{E} &= i\alpha(\kappa - i((\Delta\omega - J) - \frac{g^2}{\delta}(1 + \frac{4g^2}{\delta^2}|\alpha|^2)^{-1/2})\end{aligned} \tag{29}$$

Although the state equations provide a convenient way to demonstrate bistability, symmetry-breaking state equations are difficult to derive. Instead, the semiclassical equations must propagated from proper initial conditions to reach symmetry-breaking steady states, typically within the bistable region for small cavity coupling values. The photon numbers for these symmetry-breaking states are shifted slightly from the bistable solutions, as seen in Figure 9.

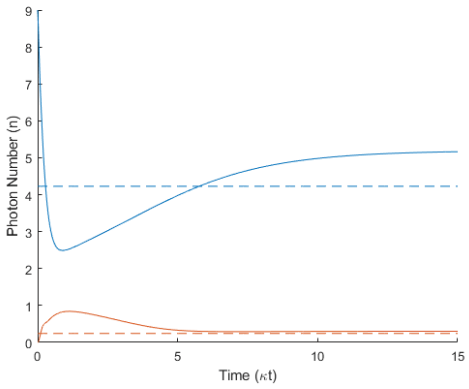

FIG. 9: Semiclassical equations propagated to steady states for $\Delta\omega/\kappa = 0$, $g/\kappa = 10$, $\mathcal{E}/\kappa = 4$, $\gamma/\kappa = 16$, $J/\kappa = 0.5$. Solid lines show propagation of $|\alpha|^2$ for cavities initialized with 9 photons (blue) and 0 photons (red). The dotted lines mark the upper (blue) and lower (red) symmetry-preserving steady states as predicted by the semiclassical equations and state equation

Although symmetry-breaking states arise from the bistable behavior of the JC model, cavity coupling effectively shifts the bistable region when symmetry is broken. The strength of the cavity coupling determines how far the bistable region shifts. As cavity coupling continues to increase, the bistable region along with its symmetry-breaking states cease to exist. Symmetry-breaking states calculated from the semiclassical equations are compared to the symmetry-preserving states predicted by the state equation in Figure 10.

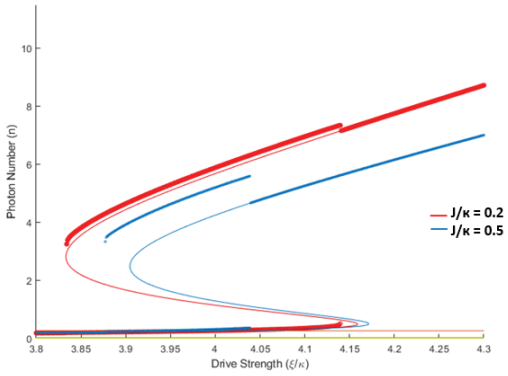

FIG. 10: Symmetry-breaking and symmetry-preserving bistability for $\Delta\omega/\kappa = 0, g/\kappa = 10, \gamma/\kappa = 16$. Thin lines were produced by the state equation to show symmetry-preserving solutions, while thick lines come from steady states of semiclassical equations with initial conditions $\alpha_1 = \sqrt{9}, \alpha_2 = 0$

As cavity coupling shifts symmetry-breaking bistability towards lower drive strengths, there exists a region where bistability can *only* be accomplished if symmetry is broken. With a cavity coupling of $J/\kappa = 0.5$, as drive strength increases the number of stable solutions goes from one (symmetry-preserving), to three (two symmetry-breaking, one symmetry-preserving), to four (two symmetry-breaking, two symmetry-preserving), to two (symmetry-preserving, and finally back to one (symmetry-preserving).

Although symmetry-breaking states can extend past the typical bistable region, these states are not present throughout the bistable region unless cavity coupling is 0, in which case the two cavity system is simply two individual, non-interacting JC cavities. As cavity coupling increases, both the bistable region and symmetry-breaking region are restricted to smaller ranges of drive strengths, but the symmetry-breaking region is restricted faster.

D. Mean Field Phase Diagram

The mean field phase diagram for the two cavity system in Figure 11 shows the regions of both symmetry-preserving and symmetry-breaking bistability. The bistability region is largest for no cavity coupling, and reaches a critical point at $J/\kappa = 1.55$, $\mathcal{E}/\kappa = 4.32$ for the parameters of Figure 11. Past this bistable region, the transition from low photon states to high photon states is still relatively sharp, but at no drive strength are two distinct states accessible. The symmetry-breaking region tends towards lower drive strengths as cavity coupling increases, and disappears altogether before the typical bistable region does.

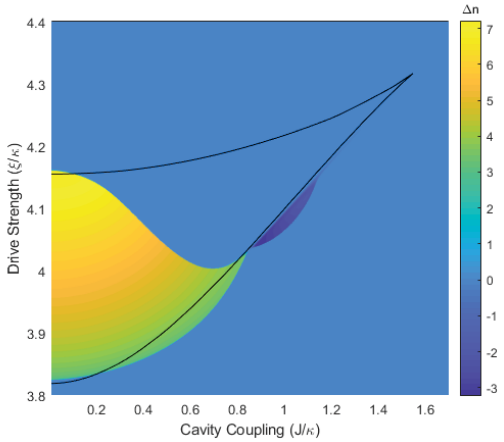

FIG. 11: Bistability phase diagram of JC dimer for $\Delta\omega/\kappa = 0, g/\kappa = 10, \gamma/\kappa = 16$. The black lines outline the bistable region when the cavities behave identically. The color plot shows the difference in photon number $\Delta n = |\alpha_1|^2 - |\alpha_2|^2$ between the steady states with initial conditions $\alpha_1 = \sqrt{9}, \alpha_2 = 0$

As discussed previously, certain cavity coupling strengths allow for symmetry-breaking steady states outside of the region for symmetric bistability. This region has two critical points, one of which locates the disappearance of symmetry-breaking states at $J/\kappa = 1.14$, $\mathcal{E}/\kappa = 4.15$. The other critical point occurs at $J/\kappa = 0.85$, $\mathcal{E}/\kappa = 4.03$ where the cavities experience flipping of photon states resulting in a negative Δn. Past this first critical point, in the dark blue region of the phase diagram, the cavities reach steady states *opposite* of their initial states. In the mean field interpretation, at some point in time the two cavities have the same number of photons but still reach steady state with broken symmetry. The propagation of the semiclassical equations in this region is shown in Figure 12.

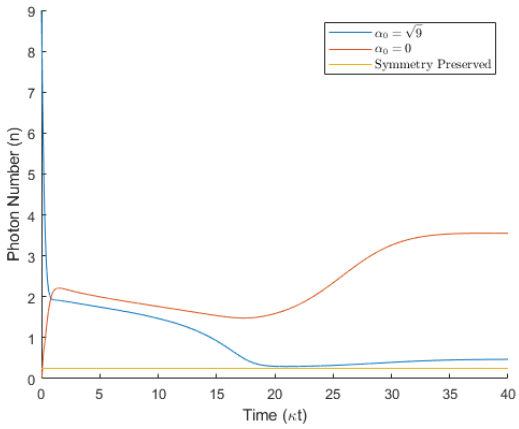

FIG. 12: Propagation of semiclassical equations demonstrating symmetry flipping for the JC dimer for $\Delta\omega/\kappa = 0$, $g/\kappa = 10$, $\gamma/\kappa = 16$. The parameters $\mathcal{E}/\kappa = 4.048$, $J/\kappa = 0.92$ place this system in the dark blue region of Figure 11.

Note that there is only one symmetry-preserving solution for the parameters used in Figure 12, as it is outside the region of bistability shown in the phase diagram. All steady states where the cavities flip from their initial conditions are only possible outside the bistable region for the JC dimer. Although the steady state Δn settles around 3 photons in Figure 12, immediately after the cavities flip high and low photon number states Δn remains small before eventually the solutions diverge. It is reasonable to expect quantum fluctuations to easily disrupt this propagation. However, there may be parameter regimes that exhibit the same symmetry flipping behavior at higher photon numbers where quantum fluctuations would not easily cause switching between solutions. This behavior is not unique to the dimer; in the three cavity system it is more pronounced and becomes a distinguishing feature, as discussed in Section VI.

E. Dispersive JC Dimer

Quantum trajectories in the dispersive regime exhibit clear symmetry-breaking behavior in the two cavity system. Just as slightly offsetting the frequencies of the cavity and atom recovers mean field bistability for the single cavity, doing so for the dimer allows for symmetry-breaking states. The trajectory shown in Figure 13 demonstrates the presence of both symmetry-preserving and symmetry-breaking states in a regime where all four solutions are considered stable.

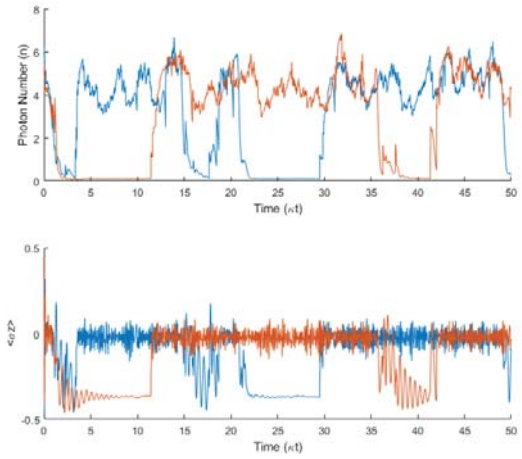

FIG. 13: Quantum trajectory for JC dimer for $\delta/\kappa = 1, \Delta\omega_c/\kappa = 3, g/\kappa = 10, \mathcal{E}/\kappa = 2.6, \gamma/\kappa = 0, J/\kappa = 0.2$. The top panel shows photon number for cavity one (blue) and cavity two (red), while the bottom panel shows the expectation value $\langle\hat{\sigma}_z\rangle$ reflecting the state of the atom

In this weak-dispersive regime ($\delta < g$), whenever the cavity is populated with photons the atom and cavity field exchange energy, causing the oscillations near $\langle\hat{\sigma}_z\rangle = 0$. In the vacuum state, there is no energy to exchange, leaving the atom close to its ground state. Therefore knowing the state of the atom also determines the state of the cavity field, and vice versa. This also means that although the atoms do not interact directly like the cavity fields, they are indirectly coupled through photon hopping. In this particular quantum trajectory, with relatively weak cavity coupling compared to atom-light coupling $J/g = 0.02$, the system happens to have broken symmetry more often than preserved. At each time step of the trajectory, the number of photons in each cavity is compared, shown in a histogram of Δn in Figure 14.

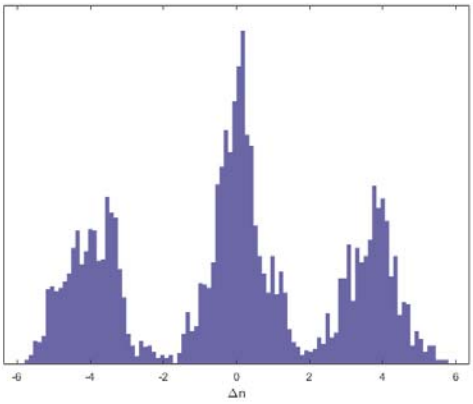

FIG. 14: Photon difference, defined as $\Delta n = n_1 - n_2$, at each time step in the quantum trajectory shown in Figure 14. An arbitrary scale is used for the vertical axes

The two side peaks in Figure 14 correspond with times during the trajectory when one cavity was in a high photon state and the other was in a low photon state. For larger cavity coupling, symmetry-breaking states are less accessible so the side peaks are not as high but their presence still indicates symmetry-breaking bistability.

Just as in the the non-dispersive case, the photon number is shifted by the cavity coupling when symmetry is broken. In this regime, however, broken symmetry shifts the upper photon number to lower values rather than higher. Analysis of the quantum trajectory in Figure 15(c) shows how the photon number is slightly shifted for symmetry-breaking states compared to symmetry-preserving ones.

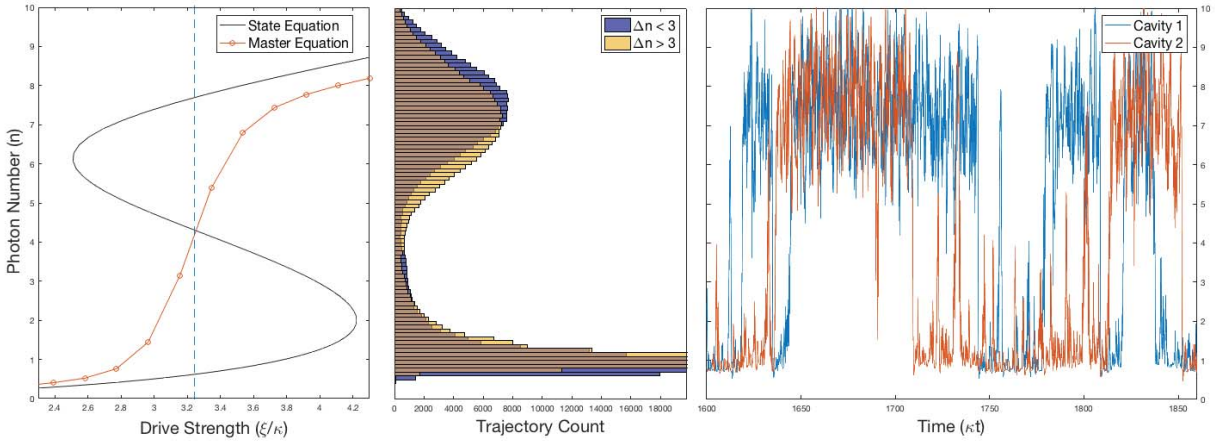

FIG. 15: (a) Semiclassical state equation compared with master equation for $\delta/\kappa = 1000$, $\Delta\omega_c/\kappa = 18$, $g/\kappa = 150$, $\gamma/\kappa = 0.084$, $J/\kappa = 0.1$ with the blue dashed line marking the drive strength used for the quantum trajectory shown in panels (b) and (c) $\mathcal{E}/\kappa = 3.21$. (b) Distribution of photon number for symmetry-preserving ($\Delta n < 3$) and symmetry-breaking ($\Delta n > 3$) states taken at each time step in the trajectory shown in panel (c). (c) Portion of a quantum trajectory for the JC dimer that shows both symmetry-preserving and symmetry-breaking states for the same parameters as panel (a) and drive strength $\mathcal{E}/\kappa = 3.21$

Although slight, there is a discernible difference in photon number between the symmetry-breaking and symmetry-preserving states for the quantum trajectory in Figure 15(c). For each time step in the quantum trajectory, the state of the system is categorized as either symmetry-preserving if $\Delta n < 3$ or symmetry-breaking if $\Delta n > 3$. The photon distribution for each is shown in Figure 15(b), demonstrating that the bistable solutions are slightly shifted for symmetry-breaking states. This shift increases with cavity coupling strength until the critical point is reached where symmetry-breaking states are no longer accessible. Just as in Figure 13, the spin state of the atoms always corresponds with the photon state of the cavity field. Although the majority of figures in this paper show only photon number, the spins have the same high and low bistable solutions, as well as symmetry-breaking states.

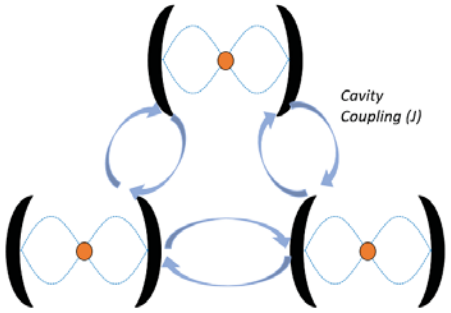

FIG. 16: Three cavity JC array, with equal rate of photon exchange between all cavities.

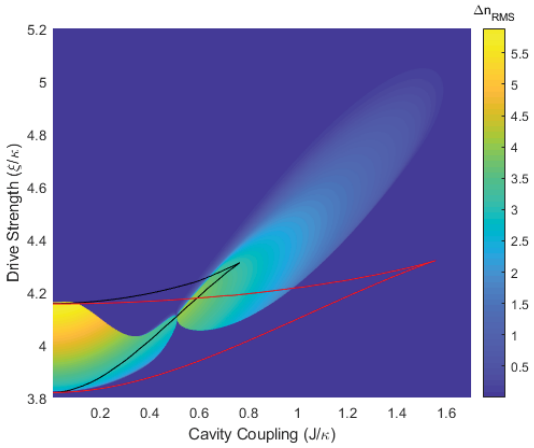

FIG. 17: Bistability phase diagram for three cavity JC model for $\Delta\omega/\kappa = 0, g/\kappa = 10, \gamma/\kappa = 16$. Black lines outline the symmetry-preserving bistability region, while the color plot shows the RMS photon difference for initial conditions $\alpha_1 = \sqrt{9}, \alpha_2 = \sqrt{9}, \alpha_3 = 0$. Red lines outline the symmetry-preserving bistability region for the two cavity system.

VI Three Cavity System

The scope of this paper extends to the three cavity JC model and how its properties might extend to a driven dissipative many body model. many body quantum systems can be studied as linear models, two dimensional arrays or three dimensional arrays. Rather than a linear model, the three cavity system considered here is arranged so that each cavity is coupled to the other two cavities, as shown in Figure 16.

The process of scaling up to the three cavity system is no different than scaling up to the two cavity system. The dimensions of the density matrix and all other operators increase to $(2N)^3$ by $(2N)^3$, making time propagation of the master equation and even wavefunctions extremely slow. The semiclassical equations become a system of 15 equations, including those for the complex conjugates α_i^* and β_i^*. This becomes the primary method of describing this system, with a focus on locating interesting parameter regimes and phase transitions to further examine with full quantum treatment.

A. Three Cavity Bistability Phase Diagram

Similar to the bistability phase diagram of the JC dimer shown in Figure 11, the semiclassical equations can be used to produce a mean field phase diagram for the three cavity system. The symmetry-preserving bistability is determined by the three cavity state equation and confirmed by time-evolution of the semiclassical equations. Since symmetry is assumed, the three cavity state equation is simply the two cavity state equation with an extra factor of 2 for the coupling term.

$$\mathcal{E} = i\alpha(\kappa - i(\Delta\omega - 2J) + \frac{g^2(\gamma/2 + i\Delta\omega)}{\gamma^2/4 + \Delta\omega^2 + 2g^2|\alpha|^2}) \tag{30}$$

The bistability of the single many body model can therefore be extended to any system of cavities as long as all cavities act identically. According to the state equation, although the size of the bistability region depends on the number of cavities each site is able to interact with, increasing the number of cavities available for interaction will never eliminate the bistability region altogether. The bistability region for a JC dimer with a cavity coupling strength of J will be the same as for a triangular array of cavities with cavity coupling strength $J/2$, or as a system that allows interactions with three other cavities with cavity coupling strength $J/3$. The critical point simply shifts to smaller cavity coupling strength values as the number of possible cavity interactions increases.

Just as before, the symmetry breaking region is determined by initializing the semiclassical equations with unequal photon numbers. In the phase diagram shown in Figure 17, two cavities are initialized near the high photon number state, $\alpha_1 = \sqrt{9}, \alpha_2 = \sqrt{9}$, and one cavity is initialized in a vacuum state $\alpha_3 = 0$. The color plot depicts the root mean squared value of the photon difference between cavities, defined as

$$\Delta n_{\mathrm{RMS}} = \sqrt{\frac{1}{3}((n_1 - n_2)^2 + (n_2 - n_3)^2 + (n_1 - n_3)^2)} \tag{31}$$

Similar to the JC dimer, the three cavity system has a region of "flipped" symmetry. The critical point near $J/\kappa = 0.5$ locates where this flipping behavior begins. Unlike the dimer, however, in the three cavity system this region extends well

past the symmetry-preserving region. In fact, the symmetry-breaking region for the three cavity system extends to the same cavity-coupling strength as the symmetry-preserving region for the dimer ($J/\kappa = 1.58$). This region can be understood as two cavities behaving as a JC dimer, while the third cavity behaves almost independently, with minimal coupling to the other cavities. This is similar to the behavior seen in the equilibrium dynamics of the JC dimer, where the atom-light coupling competed with the cavity coupling. In this parameter regime of the three cavity system, the competing coupling terms are for the two adjacent cavities.

The phase diagram in Figure 17 was produced with two cavities initialized in a high photon state ($\alpha_1 = \alpha_2 = \sqrt{9}$) and one cavity in the low photon state ($\alpha_3 = 0$). A similar but not identical diagram can be produced if one cavity is initialized in a high photon state and the other two cavities are initialized in a low photon state. The region extends to the same cavity coupling strength ($J/\kappa \approx 1.58$), but the critical point where the symmetry flipping region begins occurs at a slightly different cavity coupling strength. In fact, for all initial conditions that result in symmetry-breaking steady states, the region extends to the same vanishing critical point at $J/\kappa \approx 1.58$, but the location of the symmetry flipping critical point changes. For future research, a more comprehensive bistability phase diagram in the cavity-coupling drive-strength space should be produced where the semiclassical equations are initialized with all possible values of each α_i, forming a symmetry-breaking region that encompasses all possible drive strength and cavity coupling values.

B. Onset of Spin Frustration

The region of "flipped" symmetry is of particular interest because it indicates the potential for spin frustration in the many body model. The concept of spin frustration has been a focus of research for decades, particularly in the context of magnetic systems. For a lattice of interacting spins, depending on the geometry of the lattice it is possible for a spin to have competing interactions from adjacent spins. Consider the well-known anti-ferromagnetic Ising model on a triangular lattice such as the one discussed in this section. Each site in the Ising model is a single spin-1/2 system, limited to either a spin-up or spin-down state, rather than a coupled cavity field and spin-1/2 system as seen in the JC model. In the anti-ferromagnetic model, spins minimize their energy by aligning anti-parallel to the spin of their neighbors. A spin surrounded by sites that are spin up will orient itself as spin down, and vice versa. Frustration develops when conflicting interactions occur so that a spin site will have the same energy no matter which way it aligns. An example of spin frustration for the anti-ferromagnetic Ising model on a triangular lattice is shown in Figure 18.

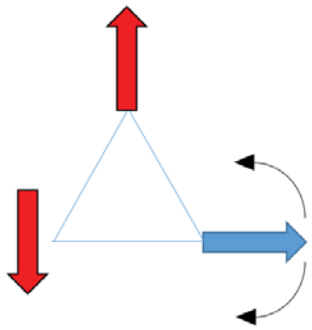

FIG. 18: Anti-ferromagnetic Ising model. Two spins have already aligned themselves anti-parallel (red), leaving the third spin in a frustrated state (blue). The spin could align either up or down, making the states degenerate.

In the JC model, either the spin state of the atom or the photon state of the cavity field could be used to study spin frustration. Considering the cavity field, the high photon number states would be spin up and low photon number states spin down. In a sense the drive strength could be compared to a magnetic field in the Ising model; for low drive strengths the cavities have a low photon number, considered spin down, and as the drive strength increases the photon number enters a bistable region where it either aligns as spin up or spin down, and eventually only aligns as spin up at high photon numbers for high drive strengths. This is not a perfect analogy to the magnetic Ising model, but could indicate something similar to spin frustration nevertheless. This makes the symmetry flipping region particularly interesting, as it is similar to anti-ferromagnetism where spins tend to align opposite each other. Such behavior is not expected for cavity fields that interact by exchanging photons; typically exchange interactions lead to systems reaching equilibrium rather than stabilize in symmetry-breaking states.

The time-evolution of the semiclassical equations in the flipped symmetry region are considered in Figure 19 in an effort to identify the onset of spin frustration in the three cavity system. The steady state solutions depend heavily on the initial conditions of the three cavities, so the initial conditions for two cavities are fixed as $\alpha_1 = 3.1$ and $\alpha_3 = 0$. This is comparable to the diagram in Figure 18, where one spin is initialized as spin up and the other as spin down, and a third spin is initialized in between with competing interactions.

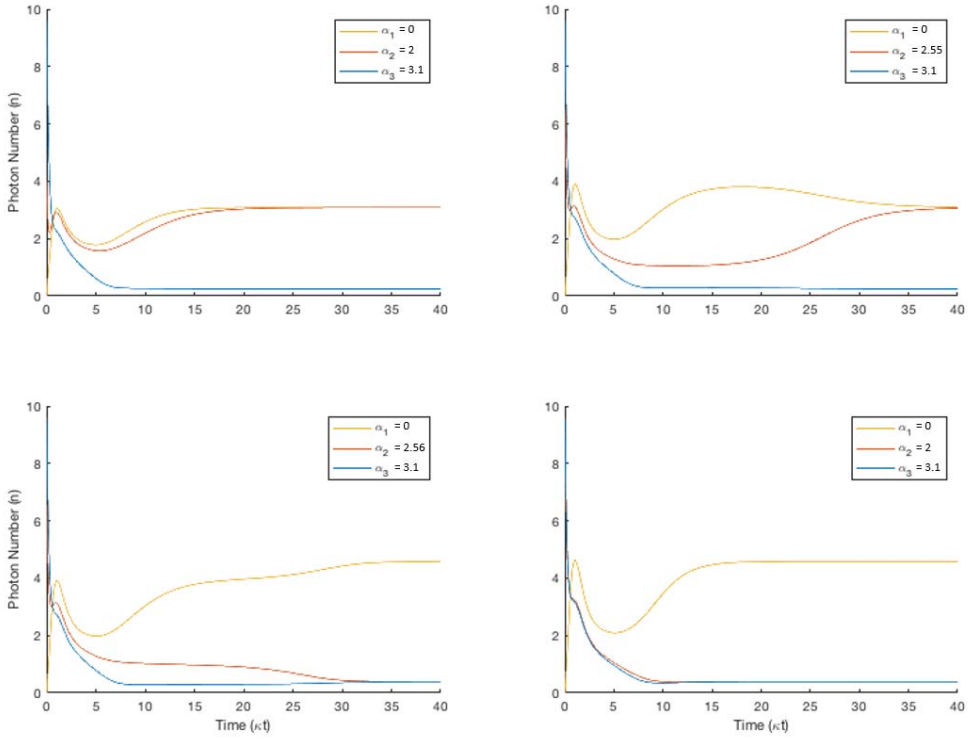

FIG. 19: Time propagation of the semiclassical equations for the three cavity system with $\Delta\omega/\kappa = 0$, $g/\kappa = 10$, $\gamma/\kappa = 16$. The parameters $\mathcal{E}/\kappa = 4.2$, $J/\kappa = 0.7$ place this system in the flipped symmetry region of the phase diagram in Figure 17. For all four panels, the equations are initialized with $\alpha_1 = 3.1, \alpha_3 = 0$. The top two panels stabilize with two cavities in high photon states, and the bottom two panels stabilize with only one cavity in a high photon state.

In addition to identical system parameters, the top-right and bottom-left panels have almost identical initial conditions. The "middle" cavity, initialized with a photon number between the other two cavities, approaches the high photon number state when initialized for all values $\alpha_2 \leq 2.55$ and approaches the low photon number state for all values $\alpha_2 \geq 2.56$. Near this critical value, the system reaches steady state slower than initial conditions near the steady states, which indicates potential spin frustration. The spin of the middle cavity can orient with either of the adjacent cavities, it just depends on which solution the cavity closer to initially.

The comparison to the Ising model is not perfect because the JC model is not a spin-1/2 system. When symmetry-breaking states are possible, rather than just two possible solutions there can be as many as six stable solutions in the three cavity system. In general three of the solutions will have a high photon number, and three will have a low photon number, with slight differences depending on the state of the other two cavities. Figure 20 shows the time propagation of the semiclassical equations to six solutions, although the three lower photon number solutions are extremely close in value.

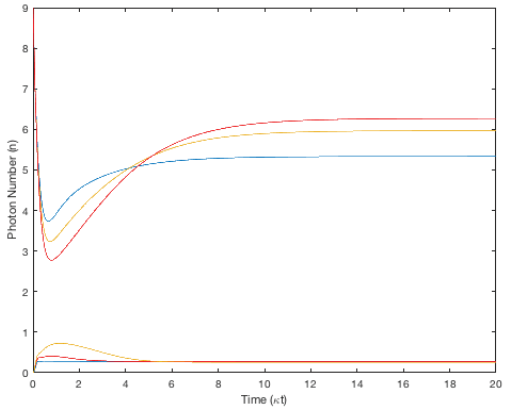

FIG. 20: Time propagation of the semiclassical equations for $\Delta\omega/\kappa = 0$, $g/\kappa = 10$, $\gamma/\kappa = 16$, $\mathcal{E}/\kappa = 4.05$, $J/\kappa = 0.2$. Symmetry-preserving (blue) and symmetry-breaking solutions for one high photon number cavity (red) and two high photon number cavities (yellow).

The three low photon number solutions are close but not equal ($n_{\text{blue}} = 0.27155$, $n_{\text{red}} = 0.2777$, $n_{\text{yellow}} = 0.2594$). A possible explanation for slightly different photon numbers is the superposition of the two bistable solutions. Although there are typically only two possible symmetry-preserving solutions, when symmetry is broken the states might be in a superposition of the high and low solutions that results in slightly different photon numbers. This can be better understood when compared to the anti-ferromagnetic Ising model again, as in Figure 21.

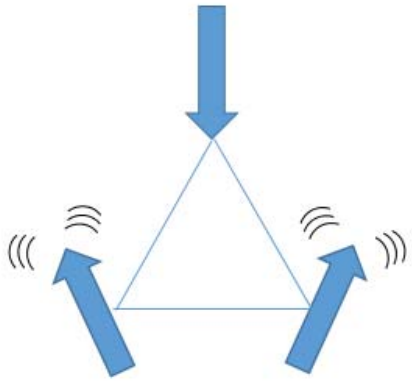

FIG. 21: Anti-ferromagnetic Ising model on triangular lattice. The two bottom spins want to align anti-parallel to the top spin, but do not want to align parallel with each other, resulting in slightly offset spin orientations

As the two bottom spins attempt to align themselves anti-parallel to their adjacent spins, they become frustrated in a state that is not truly up or down. In the JC model, full quantum treatment using the master equation could potentially demonstrate superposition of high and low photon states. Further research into the effects of coupling additional cavities in a lattice would continue to help develop the possibility of spin frustration in the many body model.

VII Conclusion

The behavior and various properties of the single Jaynes-Cummings model have been explored and then extended to the two cavity dimer and three cavity triangular array. Full quantum treatment using the Lindblad master equation and individual quantum trajectories have been compared to the semiclassical treatment to analyze regions of bistability in each system, as well as symmetry-breaking regions in the dimer and three cavity system. The dissipative quantum phase transition, understood as the breaking down of photon blockade through a cascade of multiphoton transitions in the resonant model absent of spontaneous emission, is compared to the dispersive phase transition marked by optical bistability as predicted by mean field theory. The theory of dispersive bistability in the single JC model lays the framework for understanding and identifying symmetry-breaking states for systems with multiple cavities. The two cavity dimer is considered first as a closed system, with equilibrium dynamics indicating that regions where cavity-cavity interactions dominate will not exhibit broken symmetry in the open model. This is then demonstrated in the non-equilibrium JC dimer using the same methods as those used for the single model. A bistability phase diagram comparing regions of symmetry-preserving and symmetry-breaking states is produced in the parameter space of cavity coupling and drive strength. The symmetry-breaking and symmetry-preserving states are compared using counting statistics from quantum trajectories, demonstrating how cavity coupling shifts the steady state photon number if symmetry is broken. The three cavity system is then considered primarily using semiclassical treatment, which produces a bistability phase diagram similar to that of the dimer, but with an extended region of "flipped" symmetry. This region inspired comparison of photon number states to spin states that show frustration in the context of magnetic systems, such as the anti-ferromagnetic Ising model. Propagation of the semiclassical equations in this region of flipped symmetry suggest potential spin frustration in the many body JC model.

The systems considered here are relatively simple compared to true many body models, allowing for a comprehensive understanding of the quantum behavior behind properties such as bistability and symmetry-breaking states. Further research into the extension of these properties to larger systems of Jaynes-Cummings cavities will eventually unite our understanding of the single dissipative model with the many body non-dissipative model. The physics explored in this paper can be applied in several directions for further research through exploration of all parameter spaces including detuning, atom-light coupling, cavity dissipation, and spontaneous emission. Non-equilibrium physics, particularly in quantum many body systems, remains as difficult to describe as it is important for the eventual application of quantum mechanics to information manipulation and quantum simulators. The physics presented here provides a theoretical basis for any experiments involving arrays of quantum oscillators coupled to a spin-1/2 systems.

[1] A. Daley, "Quantum trajectories and open many-body quantum systems," *Advances in Physics*, vol. 63, 2014.

[2] L. S. Bishop, J. M. Chow, J. Koch, A. A. Houck, M. H. Devoret, E. Thuneberg, S. M. Girvin, and R. J. Schoelkopf, "Nonlinear response of the vacuum rabi resonance," *Nature Physics*, vol. 5, p. 105, 2009.

[3] S. Schmidt, D. Gerace, A. A. Houck, G. Blatter, and H. E. Tureci, "Nonequilibrium delocalization-localization transition of photons in circuit quantum electrodynamics," *Physical Review B*, vol. 82, p. 100507, 2010.

[4] M. Armen, A. Miller, and H. Mabuchi, "Spontaneous dressed-state polarization in the strong driving regime of cavity qed," *Physical Review Letters*, vol. 103, p. 173601, 2009.

[5] C. Lang, D. Bozyigit, C. Eichler, L. Steffen, J. M. Fink, A. A. Abdumalikov, M. Baur, S. Filipp, M. P. da Silva, A. Blais, and A. Wallraff, "Observation of resonant photon blockade at microwave frequencies using correlation function measurements," *Physical Review Letters*, vol. 106, 2011.

[6] J. Gea-Banacloche, "Collapse and revival of the state vector in the jaynes-cummings model: An example of state preparation by a quantum apparatus," *Physical Review Letters*, vol. 65, 1990.

[7] E. Jaynes and F. Cummings, "Comparison of quantum and semiclassical radiation theories with application to the beam maser," *Proceedings of the IEEE*, vol. 51, 1963.

[8] H. J. Carmichael, "Breakdown of photon blockade: A dissipative quantum phase transition in zero dimensions," *Phys. Rev. X.*, vol. 5, p. 031028, 2015.

[9] A. Imamoglu, H. Schmidt, G. Woods, and M. Deutsh, "Strongly interacting photons in a nonlinear cavity," *Physics Review Letters*, vol. 79, p. 8, 1997.

[10] P. Alsing and H. J. Carmichael, "Spontaneous dressed-state polarization of a coupled atom and cavity mode," *Quantum Optics*, vol. 3, 1991.

[11] Mavrogordatos, P. Szafulski, E. Ginossar, and M. H. Szymanska, "Mean-field and quantum-fluctuation dynamics in the driven dispersive jaynes-cummings model," *Proceedings of the Society of Photo-Optical Instrumentation Engineers*, 2016.

[12] R. Miller, T. E. Northup, K. M. Birnbaum, A. Boca, A. D. Boozer, and H. J. Kimble, "Trapped atoms in cavity qed: Coupling quantized light and matter," *Journal of Physics B: Atomic, Molecular and Optical Physics*, vol. 38, 2005.

[13] P. Alsing and D. S. Guo, "Dynamic stark effect for the jaynes-cummings system," *Physical Review A*, vol. 45, 1992.

[14] A. Blais, R.-S. Huang, A. Wallraff, S. M. Girvin, and R. J. Schoelkopf, "Cavity quantum electrodynamics for superconducting electrical circuits: an architecture for quantum computation," *Physics Review A*, vol. 69, p. 062320, 2004.

[15] J. Raftery, D. Sadri, S. Schmidt, H. E. Tureci, and A. A. Houck, "Observation of a dissipation-induced classical to quantum transition," *Physical Review X*, vol. 4, p. 031043, 2014.

[16] M. Foss-Feig, P. Niroula, J. T. Young, M. Hafezi, A. V. Gorshkov, R. M. Wilson, and M. F. Maghrebi, "Emergent equilibrium in many-body optical bistability," *Physical Review A*, vol. 95, 2017.

[17] S. Schmidt, G. Blatter, and J. Keeling, "From the jaynes-cummings-hubbard to the dicke model," *Physical Review B*, vol. 46, p. 224020, 2013.

[18] B. Cao, K. W. Mahmud, and M. Hafezi, "Two coupled nonlinear cavities in a driven-dissipative environment," *Physical Review A*, vol. 94, p. 063805, 2016.

[19] C. Gomes, A. Souza, and F. Almeida, "Mott insulator to superfluid phase transition in bravais lattices via the jaynes-cummings-hubbard model," *European Physical Journal B*, 2012.

[20] J. Koch and K. L. Hur, "Superfluid-mott insulator transition of light in the jaynes-cummings lattice," *Physical Review A*, vol. 80, p. 023811, 2009.

[21] C. Gomes, F. Almeida, and A. Souza, "Influence of the kerr effect in a mott insulator on the superfluid transition from the point of view of the jaynes-cummings-hubbard model," *Physics Letters A*, vol. 380, pp. 1799–1803, 2016.

[22] S. Schmidt and J. Koch, "Circuit qed lattices: Towards quantum simulation with superconducting circuits," *CR Physique*, 2012.

[23] K. L. Hur, L. Henriet, A. Petrescu, K. Plekhanov, G. Roux, and M. Schiro, "Many-body quantum electrodynamics networks: Non-equilibrium condensed matter physics with light," *C.R. Physique*, vol. 17, pp. 808–835, 2016.

[24] W. Li, L. Hamadeh, and I. Lesanovsky, "Probing the interaction betwen rydberg-dressed atoms through interference," *Physical Review A*, vol. 85, p. 053615, 2012.

[25] I. Bloch, J. Dalibard, and W. Zwerger, "Many-body physics with ultracold gases," *Reviews of Modern Physics*, vol. 80, 2008.

[26] R. Jordens, N. Strohmaier, K. Gunter, H. Moritz, and T. Esslinger, "A mott insulator of fermionic atoms in an optical lattice," *Nature*, vol. 455, pp. 204–207, 2008.

[27] H. Sambe, "Steady states and quasienergies of a quantum-mechanical system in an oscillating field," *Physical Review A*, vol. 7, 1973.

Appendices

A Hamiltonian Diagonalization

The Hamiltonian can be represented as a diagonalizable matrix where the diagonal elements of the matrix are the energy values for each configuration of the system. The Hamiltonian must encompass the entire Hilbert space of the system, which contains all possible states of the system. The Hamiltonian is then a $(2N)^m$ by $(2N)^m$ matrix. The Hamiltonian is the sum of all sub-Hamiltonians, so that $\hat{H} = \sum_{n=0}^{N} h_n$ where

$$h_n = \begin{bmatrix} \langle n,\downarrow|H|n,\downarrow\rangle & \langle n,\downarrow|H|n-1,\uparrow\rangle \\ \langle n-1,\uparrow|H|n,\downarrow\rangle & \langle n-1,\uparrow|H|n-1,\uparrow\rangle \end{bmatrix} \tag{32}$$

Using the Hamiltonian from Eq. (1), each sub-Hamiltonian becomes

$$h_n = \hbar \begin{bmatrix} \omega_0 n & g\sqrt{n} \\ g\sqrt{n} & \omega_0 n \end{bmatrix} \tag{33}$$

In order to diagonalize the Hamiltonian, the eigenvalues, λ, of each sub-Hamiltonian must be found.

$$\begin{aligned} \det \begin{bmatrix} \omega_0 n - \lambda & g\sqrt{n} \\ g\sqrt{n} & \omega_0 n - \lambda \end{bmatrix} = 0 &= (\omega_0 n - \lambda)^2 - g^2 n \\ (\lambda - \omega_0 n)^2 &= g^2 n \\ \lambda_\pm &= \omega_0 n \pm g\sqrt{n} \end{aligned} \tag{34}$$

These eigenvalues are the energy doublets associated with each set of eigenstates. The eigenvectors are then found:

$$\begin{aligned} \begin{bmatrix} \omega_0 n - \lambda & g\sqrt{n} \\ g\sqrt{n} & \omega_0 n - \lambda \end{bmatrix} \begin{bmatrix} x_1 \\ x_2 \end{bmatrix} &= \begin{bmatrix} 0 \\ 0 \end{bmatrix} \\ \hbar g\sqrt{n} \begin{bmatrix} \pm 1 & 1 \\ 1 & \pm 1 \end{bmatrix} \begin{bmatrix} x_1 \\ x_2 \end{bmatrix} &= \begin{bmatrix} 0 \\ 0 \end{bmatrix} \end{aligned} \tag{35}$$

$$\vec{x}_\pm = \begin{bmatrix} x_1 \\ x_2 \end{bmatrix} = \frac{1}{\sqrt{2}} \begin{bmatrix} 1 \\ \pm 1 \end{bmatrix} \tag{36}$$

Therefore the eigenstates for the system are

$$\begin{aligned} &|E_{n,\pm}\rangle = \frac{1}{\sqrt{2}}(|n,\downarrow\rangle \pm |n-1,\uparrow\rangle) \\ &\text{with energies: } E_{n,\pm} = n\hbar\omega_0 \pm \sqrt{n}\hbar g \end{aligned} \tag{37}$$

To complete the diagonalization of each h_n, a matrix C is formed by the eigenvectors $\vec{x}_\pm$ so that $D_n = C^{-1} h_n C$

$$\begin{aligned} D_n &= \frac{\hbar}{2} \begin{bmatrix} 1 & 1 \\ 1 & -1 \end{bmatrix} \begin{bmatrix} \omega_0 n & g\sqrt{n} \\ g\sqrt{n} & \omega_0 n \end{bmatrix} \begin{bmatrix} 1 & 1 \\ 1 & -1 \end{bmatrix} \\ D_n &= \begin{bmatrix} n\hbar\omega_0 - \sqrt{n}\hbar g & 0 \\ 0 & n\hbar\omega_0 + \sqrt{n}\hbar g \end{bmatrix} \end{aligned} \tag{38}$$

The diagonalized matrix, $D = \sum_{n=0}^{N} D_n$, can then be used to read off energy levels and determine the lowest energy state, i.e. the ground state.

B Single Cavity Semiclassical Equations

A. Necessary Equations

1. Driven Jaynes-Cummings Cavity Hamiltonian

$$\hat{H}_{JC} = \hbar\Delta\omega_a\hat{\sigma}^+\hat{\sigma}^- + \hbar\Delta\omega_c\hat{a}^\dagger\hat{a} + \hbar g(\hat{a}^\dagger\hat{\sigma}^- + \hat{a}\hat{\sigma}^+) + \hbar\mathcal{E}(\hat{a}^\dagger + \hat{a}) \tag{39}$$

2. Lindblad Master Equation

$$\dot{\rho} = \frac{1}{i\hbar}\big[\hat{H}_{JC}, \rho] + \kappa(2\hat{a}\rho\hat{a}^\dagger - \hat{a}^\dagger\hat{a}\rho - \rho\hat{a}^\dagger\hat{a}) + 2\gamma(2\hat{\sigma}^-\rho\hat{\sigma}^+ - \hat{\sigma}^+\hat{\sigma}^-\rho - \rho\hat{\sigma}^+\hat{\sigma}^-) \tag{40}$$

B. Equation of Motion for $\alpha = \langle\hat{a}\rangle$

$$\dot{\alpha} = \mathrm{Tr}[\dot{\rho}\hat{a}] = \frac{1}{i\hbar}\mathrm{Tr}\big[[\hat{H}_{JC}, \rho]\hat{a}\big] + \mathrm{Tr}[\kappa(2\hat{a}\rho\hat{a}^\dagger - \hat{a}^\dagger\hat{a}\rho - \rho\hat{a}^\dagger\hat{a})\hat{a}] + \mathrm{Tr}[2\gamma(2\hat{\sigma}^-\rho\hat{\sigma}^+ - \hat{\sigma}^+\hat{\sigma}^-\rho - \rho\hat{\sigma}^+\hat{\sigma}^-)\hat{a}] \tag{41}$$

$$\begin{aligned}\frac{1}{i\hbar}\mathrm{Tr}\big[[\hat{H}_{JC}, \rho]\hat{a}\big] = -i\mathrm{Tr}\big[&\Delta\omega_a[\hat{\sigma}^+\hat{\sigma}^-, \rho]\hat{a} + \Delta\omega_c[\hat{a}^\dagger\hat{a}, \rho]\hat{a} \\ &+ g[\hat{a}^\dagger\hat{\sigma}^-, \rho]\hat{a} + g[\hat{a}\hat{\sigma}^+, \rho]\hat{a} + \mathcal{E}[\hat{a}^\dagger, \rho]\hat{a} + \mathcal{E}[\hat{a}, \rho]\hat{a}\big]\end{aligned} \tag{42}$$

Looking at just the $\Delta\omega$ terms:

$$i\mathrm{Tr}[\Delta\omega_a(\hat{\sigma}^+\hat{\sigma}^-\rho\hat{a} - \rho\hat{\sigma}^+\hat{\sigma}^-\hat{a}) + \Delta\omega_c(\hat{a}^\dagger\hat{a}\rho\hat{a} - \rho\hat{a}^\dagger\hat{a}\hat{a})] \tag{43}$$

$$\begin{aligned}[\hat{a}, \hat{a}^\dagger] &= 1 \\ \hat{a}\hat{a}^\dagger &= \hat{a}^\dagger\hat{a} + 1\end{aligned} \tag{44}$$

The $\Delta\omega_a$ terms cancel because the annihilation operator $\hat{a}$ commutes with the spin operators $\hat{\sigma}^-$ and $\hat{\sigma}^+$, which makes the first two terms equivalent. We are then left with:

$$\begin{aligned}i\Delta\omega_c\mathrm{Tr}[\hat{a}\hat{a}^\dagger\hat{a}\rho - \hat{a}^\dagger\hat{a}\hat{a}\rho] \\ i\Delta\omega_c\mathrm{Tr}[(\hat{a}^\dagger\hat{a} + 1)\hat{a}\rho - \hat{a}^\dagger\hat{a}\hat{a}\rho] \\ i\Delta\omega_c\mathrm{Tr}[\hat{a}\rho] = \boxed{i\Delta\omega\alpha}\end{aligned} \tag{45}$$

Looking at just the g terms:

$$-ig\mathrm{Tr}[\hat{a}^\dagger\hat{\sigma}^-\rho\hat{a} - \rho\hat{a}^\dagger\hat{\sigma}^-\hat{a} + \hat{a}\hat{\sigma}^+\rho\hat{a} - \rho\hat{a}\hat{\sigma}^+\hat{a}] \tag{46}$$

Once again, the last two terms cancel because the $\hat{a}$ and $\hat{\sigma}^-$ operators commute. This leaves the g terms as:

$$\begin{aligned}-ig\mathrm{Tr}[\hat{a}\hat{a}^\dagger\hat{\sigma}^-\rho - \hat{a}^\dagger\hat{\sigma}^-\hat{a}\rho] \\ -ig\mathrm{Tr}[\hat{a}\hat{a}^\dagger\hat{\sigma}^-\rho - \hat{a}^\dagger\hat{a}\hat{\sigma}^-\rho] \\ -ig\mathrm{Tr}[(\hat{a}^\dagger\hat{a} + 1)\hat{\sigma}^-\rho - \hat{a}^\dagger\hat{a}\hat{\sigma}^-\rho)] \\ -ig\mathrm{Tr}[\hat{\sigma}^-\rho] = \boxed{-ig\beta}\end{aligned} \tag{47}$$

Where $\beta = \langle\hat{\sigma}^-\rangle = \mathrm{Tr}[\hat{\sigma}^-\rho]$
Next, looking at just the $\mathcal{E}$ terms:

$$\begin{aligned}-i\mathcal{E}\mathrm{Tr}[\hat{a}^\dagger\rho\hat{a} - \rho\hat{a}^\dagger\hat{a} + \hat{a}\rho\hat{a} - \rho\hat{a}\hat{a}] \\ -i\mathcal{E}\mathrm{Tr}[(\hat{a}^\dagger\hat{a} + 1)\rho - \hat{a}^\dagger\hat{a}\rho] \\ -i\mathcal{E}\mathrm{Tr}[\rho] = \boxed{-i\mathcal{E}}\end{aligned} \tag{48}$$

The cavity loss terms become:

$$\begin{aligned}\kappa\mathrm{Tr}[2\hat{a}\rho\hat{a}^\dagger\hat{a} - \hat{a}^\dagger\hat{a}\rho\hat{a} - \rho\hat{a}^\dagger\hat{a}\hat{a}] \\ \kappa\mathrm{Tr}[2\hat{a}^\dagger\hat{a}\hat{a}\rho - \hat{a}\hat{a}^\dagger\hat{a}\rho - \hat{a}^\dagger\hat{a}\hat{a}\rho] \\ \kappa\mathrm{Tr}[\hat{a}^\dagger\hat{a}\hat{a}\rho - (1+\hat{a}^\dagger\hat{a})\hat{a}\rho] \\ \kappa\mathrm{Tr}[-\hat{a}\rho] = \boxed{-\kappa\alpha}\end{aligned} \tag{49}$$

Finally the spontaneous emission terms all cancel because the only operators are spin operators, which always commute with $\hat{a}$. Combining the terms for $\Delta\omega_c, g, \mathcal{E}$, and κ, the equation of motion for $\dot{\alpha}$ is:

$$\boxed{\dot{\alpha} = (i\Delta\omega_c - \kappa)\alpha - ig\beta - i\mathcal{E}} \tag{50}$$

C. Equation of Motion for $\beta = \langle\hat{\sigma}^-\rangle$

$$\dot{\beta} = \mathrm{Tr}[\dot{\rho}\hat{\sigma}^-] = \frac{1}{i\hbar}\mathrm{Tr}\big[[\hat{H}_{JC},\rho]\hat{\sigma}^-\big] + \mathrm{Tr}[\kappa(2\hat{a}\rho\hat{a}^\dagger - \hat{a}^\dagger\hat{a}\rho - \rho\hat{a}^\dagger\hat{a})\hat{\sigma}^-] + \mathrm{Tr}[2\gamma(2\hat{\sigma}^-\rho\hat{\sigma}^+ - \hat{\sigma}^+\hat{\sigma}^-\rho - \rho\hat{\sigma}^+\hat{\sigma}^-)\hat{\sigma}^-] \tag{51}$$

$$\begin{aligned}\frac{1}{i\hbar}\mathrm{Tr}\big[[\hat{H}_{JC},\rho]\hat{\sigma}^-\big] = -i\mathrm{Tr}\big[&\Delta\omega_a[\hat{\sigma}^+\hat{\sigma}^-,\rho]\hat{\sigma}^- + \Delta\omega_c[\hat{a}^\dagger\hat{a},\rho]\hat{\sigma}^- \\ &+ g[\hat{a}^\dagger\hat{\sigma}^-,\rho]\hat{\sigma}^- + g[\hat{a}\hat{\sigma}^+,\rho]\hat{\sigma}^- + \mathcal{E}[\hat{a}^\dagger,\rho]\hat{\sigma}^- + \mathcal{E}[\hat{a},\rho]\hat{\sigma}^-\big]\end{aligned} \tag{52}$$

Again, separating the terms out by their coefficient, the $\Delta\omega$ terms are:

$$i\mathrm{Tr}[\Delta\omega_a(\hat{\sigma}^+\hat{\sigma}^-\rho\hat{\sigma}^- - \rho\hat{\sigma}^+\hat{\sigma}^-\hat{\sigma}^-) + \Delta\omega_c(\hat{a}^\dagger\hat{a}\rho\hat{\sigma}^- - \rho\hat{a}^\dagger\hat{a}\hat{\sigma}^-)] \tag{53}$$

The $\Delta\omega_c$ terms cancel because the annihilation and reation operators $\hat{a}$ and $\hat{a}^\dagger$ don't commute with the $\hat{\sigma}^-$ operator. Some relationships for spin operators will be useful throughout the rest of the derivation

$$\sigma_x = \begin{bmatrix}0 & 1\\ 1 & 0\end{bmatrix} \quad \sigma_y = \begin{bmatrix}0 & -i\\ i & 0\end{bmatrix} \quad \sigma_z = \begin{bmatrix}1 & 0\\ 0 & -1\end{bmatrix} \tag{54}$$

$$\hat{\sigma}^+ = \sigma_x + i\sigma_y = \begin{bmatrix}0 & 1\\ 0 & 0\end{bmatrix} \quad \hat{\sigma}^- = \sigma_x - i\sigma_y = \begin{bmatrix}0 & 0\\ 1 & 0\end{bmatrix} \tag{55}$$

$$[\hat{\sigma}^+,\hat{\sigma}^-] = \sigma_z \tag{56}$$

Considering the $\Delta\omega_a$ terms again:

$$\begin{aligned}i\Delta\omega_a\mathrm{Tr}[\hat{\sigma}^-\hat{\sigma}^+\hat{\sigma}^-\rho - \hat{\sigma}^+\hat{\sigma}^-\hat{\sigma}^-\rho] \\ -i\Delta\omega_a\mathrm{Tr}\big[[\hat{\sigma}^+,\hat{\sigma}^-]\hat{\sigma}^-\rho\big] \\ -i\Delta\omega_a\mathrm{Tr}[\sigma_z\hat{\sigma}^-\rho]\end{aligned} \tag{57}$$

$$\sigma_z\hat{\sigma}^- = \begin{bmatrix}1 & 0\\ 0 & -1\end{bmatrix}\begin{bmatrix}0 & 0\\ 1 & 0\end{bmatrix} = \begin{bmatrix}0 & 0\\ -1 & 0\end{bmatrix} = -\hat{\sigma}^- \tag{58}$$

$$i\Delta\omega\mathrm{Tr}[\hat{\sigma}^-\rho] = \boxed{i\Delta\omega\beta} \tag{59}$$

Looking at the g terms:

$$\begin{aligned} -ig\mathrm{Tr}[\hat{a}^\dagger\hat{\sigma}^-\rho\hat{\sigma}^- - \rho\hat{a}^\dagger\hat{\sigma}^-\hat{\sigma}^- + \hat{a}\hat{\sigma}^+\rho\hat{\sigma}^- - \rho\hat{a}\hat{\sigma}^+\hat{\sigma}^-] \\ -ig\mathrm{Tr}[\hat{a}^\dagger\hat{\sigma}^-\hat{\sigma}^-\rho - \hat{a}^\dagger\hat{\sigma}^-\hat{\sigma}^- + \hat{\sigma}^-\hat{\sigma}^+\hat{a}\rho - \hat{\sigma}^+\hat{\sigma}^-\hat{a}\rho] \\ ig\mathrm{Tr}\big[[\hat{\sigma}^+,\hat{\sigma}^-]\hat{a}\rho\big] = ig\mathrm{Tr}[\sigma_z\hat{a}\rho] = \boxed{ig\alpha\zeta} \end{aligned} \tag{60}$$

Where $\zeta = \langle\sigma_z\rangle$.

Both the drive terms and cavity loss terms are 0 because the only have photon creation and annihilation operators which always commute with $\hat{\sigma}^-$. Finally, the spontaneous emission terms become:

$$\begin{aligned} \gamma/2\mathrm{Tr}[2\hat{\sigma}^-\rho\hat{\sigma}^+\hat{\sigma}^- - \hat{\sigma}^+\hat{\sigma}^-\rho\hat{\sigma}^- - \rho\hat{\sigma}^+\hat{\sigma}^-\hat{\sigma}^-] \\ \gamma/2\mathrm{Tr}[2\hat{\sigma}^+\hat{\sigma}^-\hat{\sigma}^-\rho - \hat{\sigma}^-\hat{\sigma}^+\hat{\sigma}^-\rho - \hat{\sigma}^+\hat{\sigma}^-\hat{\sigma}^-\rho] \\ \gamma/2\mathrm{Tr}\big[[\hat{\sigma}^+\hat{\sigma}^-]\hat{\sigma}^-\rho] = \gamma/2\mathrm{Tr}[\hat{\sigma}_z\hat{\sigma}^-\rho] \end{aligned} \tag{61}$$

Where the spin operator relation $\hat{\sigma}_z\hat{\sigma}^- = -\hat{\sigma}^-$ leaves us with

$$-\gamma/2\mathrm{Tr}[\hat{\sigma}^-\rho] = -\frac{\gamma}{2}\beta \tag{62}$$

This leaves us with the equation of motion for β as

$$\boxed{\dot{\beta} = -i(\frac{\gamma}{2} - \Delta\omega_a)\beta + ig\alpha\zeta} \tag{63}$$

D. Equation of Motion for $\zeta = \langle\sigma_z\rangle$

$$\dot{\zeta} = \mathrm{Tr}[\dot{\rho}\sigma_z] = \frac{1}{i\hbar}\mathrm{Tr}\big[[\hat{H}_{JC},\rho]\sigma_z\big] + \mathrm{Tr}[\kappa(2\hat{a}\rho\hat{a}^\dagger - \hat{a}^\dagger\hat{a}\rho - \rho\hat{a}^\dagger\hat{a})\sigma_z] + \mathrm{Tr}[2\gamma(2\hat{\sigma}^-\rho\hat{\sigma}^+ - \hat{\sigma}^+\hat{\sigma}^-\rho - \rho\hat{\sigma}^+\hat{\sigma}^-)\hat{\sigma}_z] \tag{64}$$

$$\begin{aligned} \frac{1}{i\hbar}\mathrm{Tr}\big[[\hat{H}_{JC},\rho]\sigma_z\big] = -i\mathrm{Tr}\big[\Delta\omega_a[\hat{\sigma}^+\hat{\sigma}^-,\rho]\sigma_z + \Delta\omega_c[\hat{a}^\dagger\hat{a},\rho]\sigma_z \\ +g[\hat{a}^\dagger\hat{\sigma}^-,\rho]\sigma_z + g[\hat{a}\hat{\sigma}^+,\rho]\sigma_z + \mathcal{E}[\hat{a}^\dagger,\rho]\sigma_z + \mathcal{E}[\hat{a},\rho]\sigma_z\big] \end{aligned} \tag{65}$$

Looking at only the $\Delta\omega$ terms:

$$\begin{aligned} i\mathrm{Tr}[\Delta\omega_a(\hat{\sigma}^+\hat{\sigma}^-\rho\sigma_z - \rho\hat{\sigma}^+\hat{\sigma}^-\sigma_z) + \Delta\omega_c(\hat{a}^\dagger\hat{a}\rho\sigma_z - \rho\hat{a}^\dagger\hat{a}\sigma_z)] \\ i\Delta\omega_a\mathrm{Tr}[\sigma_z\hat{\sigma}^+\hat{\sigma}^-\rho - \hat{\sigma}^+\hat{\sigma}^-\sigma_z\rho] = \boxed{0} \end{aligned} \tag{66}$$

If you work through the matrix multiplication, $\sigma_z\hat{\sigma}^+\hat{\sigma}^- = \hat{\sigma}^+\hat{\sigma}^-\sigma_z$ which means the $\Delta\omega_c$ terms cancel (along with the $\Delta\omega_a$ terms which cancelled because the photon operators and spin operators don't commute). Next we look at the g terms:

$$\begin{aligned} -ig\mathrm{Tr}[\hat{a}^\dagger\hat{\sigma}^-\rho\sigma_z - \rho\hat{a}^\dagger\hat{\sigma}^-\sigma_z + \hat{a}\hat{\sigma}^+\rho\sigma_z - \rho\hat{a}\hat{\sigma}^+\sigma_z] \\ -ig\mathrm{Tr}[\sigma_z\hat{\sigma}^-\hat{a}^\dagger\rho - \hat{\sigma}^-\sigma_z\hat{a}^\dagger\rho + \sigma_z\hat{\sigma}^+\hat{a}\rho - \hat{\sigma}^+\sigma_z\hat{a}\rho] \\ -ig\mathrm{Tr}\big[[\sigma_z,\hat{\sigma}^-]\hat{a}^\dagger\rho + [\sigma_z,\hat{\sigma}^+]\hat{a}\rho\big] \end{aligned} \tag{67}$$

Knowing the following:

$$[\sigma_z,\hat{\sigma}^+] = 2\hat{\sigma}^+ \quad [\sigma_z,\hat{\sigma}^-] = -2\hat{\sigma}^- \tag{68}$$

Simplifies the g terms to

$$-2ig\mathrm{Tr}[\hat{\sigma}^+\hat{a}\rho - \hat{\sigma}^-\hat{a}^\dagger\rho] = \boxed{2ig(\alpha^*\beta - \alpha\beta^*)} \tag{69}$$

Remembering that $\alpha^* = \mathrm{Tr}[\hat{a}^\dagger\rho]$ and $\beta^* = \mathrm{Tr}[\hat{\sigma}^+\rho]$ Since combinations of σ_z and the $\hat{a}$ and $\hat{a}^\dagger$ operators can be permuted in any way, the $\mathcal{E}$ and κ terms cancel out to 0 just like for the $\dot{\beta}$ equation. The spontaneous emission terms become

$$\begin{aligned}
\gamma/2\mathrm{Tr}[2\hat{\sigma}^-\rho\hat{\sigma}^+\hat{\sigma}_z - \hat{\sigma}^+\hat{\sigma}^-\rho\hat{\sigma}_z - \rho\hat{\sigma}^+\hat{\sigma}^-\hat{\sigma}_z] \\
\gamma/2\mathrm{Tr}[2\hat{\sigma}^+\hat{\sigma}_z\hat{\sigma}^-\rho - \hat{\sigma}_z\hat{\sigma}^+\hat{\sigma}^-\rho - \hat{\sigma}^+\hat{\sigma}^-\hat{\sigma}_z\rho] \\
\gamma/2\mathrm{Tr}\big[[\hat{\sigma}^+,\hat{\sigma}_z]\hat{\sigma}^-\rho + [\hat{\sigma}_z,\hat{\sigma}^-]\rho\hat{\sigma}^-\big] \\
\gamma/2\mathrm{Tr}[-2\hat{\sigma}^+\hat{\sigma}^-\rho - 2\hat{\sigma}^+\hat{\sigma}^-\rho] = -\gamma\mathrm{Tr}[2\hat{\sigma}^+\hat{\sigma}^-\rho]
\end{aligned} \tag{70}$$

Recognizing that $\hat{\sigma}^+\hat{\sigma}^- = 1/2(\hat{\sigma}_z + 1)$,

$$-\gamma\mathrm{Tr}[(\hat{\sigma}_z + 1)\rho] = -\gamma(\zeta + 1) \tag{71}$$

The equation of motion for ζ is therefore

$$\boxed{\dot{\zeta} = -\gamma(\zeta + 1) + 2ig(\alpha^*\beta - \alpha\beta^*)} \tag{72}$$

The final system of equations derived from mean field theory are

$$\boxed{\dot{\alpha} = -(\kappa - i\Delta\omega_c)\alpha - ig\beta - i\mathcal{E}} \tag{73a}$$

$$\boxed{\dot{\beta} = -i(\frac{\gamma}{2} - \Delta\omega_a)\beta + ig\alpha\zeta} \tag{73b}$$

$$\boxed{\dot{\zeta} = -\gamma(\zeta + 1) + 2ig(\alpha^*\beta - \alpha\beta^*)} \tag{73c}$$

C Glossary

$\Delta\omega_c$: Detuning between frequency of the drive source and frequency of the photons in the cavity. Can be thought of as the difference in color of the two lights

$\Delta\omega_a$: Detuning between frequency of the drive source and frequency associated with the energy difference between the two spins of the atom

$\Delta\omega$: Drive detuning, used for simplicity when $\Delta\omega_c = \Delta\omega_a$

δ: Detuning between the frequency of the cavity field and frequency associated with the energy difference between the two spins of the atom. Large values of δ prevents exchanges of energy between the cavity field and atom

g: Atom-light coupling coefficient, reflects the likelihood of the atom and light in the cavity interacting through the emission/absorption of photons

$\mathcal{E}$: Drive Coefficient, reflects the strength of the external laser. Controls the rate at which photons are pumped into the system

Hilbert Space: contains all possible states of the system, with all combinations of photon number and spin. The Hilbert Space for a many body JC model with m cavities with a maximum of n photons each is $(2n)^m$

$|n, s\rangle$: Notation to describe the system with n photons and the atom in the s state

Hamiltonian: Mathematical description of the total energy of a system. The eigenvalues of the Hamiltonian matrix can be solved exactly in equilibrium physics, making it possible to find the ground state of the system.

$\hat{a}$ and **$\hat{a}^\dagger$**: Annihilation and creation operators for photons in the cavity

$$\begin{aligned}
\hat{a}|n, s\rangle &= \sqrt{n}|n-1, s\rangle \\
\hat{a}^\dagger|n, s\rangle &= \sqrt{n+1}|n+1, s\rangle
\end{aligned} \tag{74}$$

$\hat{\boldsymbol{\sigma}}^{+}$ and $\hat{\boldsymbol{\sigma}}^{-}$: Raising and lowering operators for the two-level atom

$$\begin{aligned} \hat{\sigma}_{-}|n,+\frac{1}{2}\rangle &= |n,-\frac{1}{2}\rangle \\ \hat{\sigma}_{+}|n,-\frac{1}{2}\rangle &= |n,+\frac{1}{2}\rangle \end{aligned} \tag{75}$$

Photon Blockade: Purely quantum mechanical effect where the absorption of one photon by the cavity blocks the absorption of a second photon. This can be extended to a multiphoton blockade, and the affect is broadened with drive and dissipation.

Density Matrix: ρ, matrix describing the state of the system, typically used for open and dissipative systems. Taking the trace of an operator acting on the density matrix returns an expectation value. The density matrix describes a statistical average of an ensemble of identical systems.

$$\hat{\rho} = |n,s\rangle\langle n,s| \tag{76}$$

Expectation Value: The probabilistic expected value of a characteristic of the system. Essentially a weighted average of all possible values, where the weight is the probability of each value.

Master Equation: Used to study the time evolution of a quantum system interacting with the environment by accounting for dissipation. Evolves the density matrix in time.

Steady State Solution: Non-equilibrium equivalent of the ground state of a system. This is the state that the a system tends towards and then remains at once reached.

$\boldsymbol{\kappa}$: Dissipation coefficient for cavity loss, reflecting the rate at which photons escape the cavity

$\boldsymbol{\gamma}$: Dissipation coefficient for spontaneous emission, reflecting the rate at which the atom emits photons outside the cavity

$\boldsymbol{J}$: Cavity coupling coefficient, reflects the rate of photon exchange between the cavities

Z: Photon Imbalance, reflecting the photon distribution in the two-cavity system. Imbalance is defined so that if the cavity one has more photons than cavity two, imbalance is positive. If cavity two has more photons than cavity one, imbalance is negative. If the cavities have the exact same number of photons, imbalance is 0.

$\boldsymbol{g_{crit}}$: critical value of atom-light coupling coefficient that marks a dynamical phase transition. Above g_{crit}, photons are essentially trapped in their local cavity, with long switching times between cavities. Below g_{crit}, photons are delocalized, as inter-cavity coupling dominates.

Symmetry-breaking State: A steady state solution to a system with multiple bodies with identical parameters where all observables of the system are not identical

Superfluid Phase: In the context of the Jaynes-Cummings model, superfluid properties include delocalization of photons that can flow freely through a lattice of cavities.

Mott-Insulator Phase: An integer number of photons are localized in their respective cavity.

Ising Model: Mathematical model of ferromagnetism for interacting spins arranged in a lattice. One of the simplest statistical models with a phase transition